

Shedding light on non-Ising polar domain walls: Insight from second harmonic generation microscopy and polarimetry analysis


Cite as: J. Appl. Phys. **129**, 081101 (2021); <https://doi.org/10.1063/5.0037286>

Submitted: 12 November 2020 • Accepted: 04 February 2021 • Published Online: 23 February 2021

 Salia Cherifi-Hertel,  Cédric Voulot,  Ulises Acevedo-Salas, et al.

COLLECTIONS

Paper published as part of the special topic on [Domains and Domain Walls in Ferroic Materials](#)

 This paper was selected as Featured



View Online



Export Citation



CrossMark

ARTICLES YOU MAY BE INTERESTED IN

[Domains and domain walls in ferroic materials](#)

Journal of Applied Physics **129**, 230401 (2021); <https://doi.org/10.1063/5.0057144>

[Characterization of ferroelectric domain walls by scanning electron microscopy](#)

Journal of Applied Physics **128**, 191102 (2020); <https://doi.org/10.1063/5.0029284>

[Negative capacitance effects in ferroelectric heterostructures: A theoretical perspective](#)

Journal of Applied Physics **129**, 080901 (2021); <https://doi.org/10.1063/5.0038971>

Lock-in Amplifiers
up to 600 MHz



Zurich
Instruments



Shedding light on non-Ising polar domain walls: Insight from second harmonic generation microscopy and polarimetry analysis

Cite as: J. Appl. Phys. **129**, 081101 (2021); doi: [10.1063/5.0037286](https://doi.org/10.1063/5.0037286)

Submitted: 12 November 2020 · Accepted: 4 February 2021 ·

Published Online: 23 February 2021



Salia Cherifi-Hertel,^{a)}  Cédric Voulot,  Ulises Acevedo-Salas,  Yide Zhang,  Olivier Crégut, Kokou Dodzi Dorkenoo, and Riccardo Hertel 

AFFILIATIONS

Université de Strasbourg, CNRS, Institut de Physique et Chimie des Matériaux de Strasbourg, UMR 7504, Strasbourg 67000, France

Note: This paper is part of the Special Topic on Domains and Domain Walls in Ferroc Materials.

^{a)} **Author to whom correspondence should be addressed:** Salia.Cherifi@ipcms.unistra.fr

ABSTRACT

Polar domain walls are currently at the focus of intensive research owing to their unusual and highly localized functional properties, which bear great potential for technological applications. They can present unusual topological features, like swirling polar structures or defect lines. The prediction of possible non-Ising and chiral internal structures of polar domain walls has been a particularly important development in this topic over the past years. This Tutorial highlights the capabilities of non-linear optics to probe these newly discovered aspects in polar non-Ising type domain walls through the second-harmonic generation (SHG) process. Fundamental symmetry properties of domain walls are presented in the context of recent advances on chiral and abnormal polar structures. We introduce the basics of the SHG and its ability to probe the symmetry down to the nanoscale, and we explain how to obtain insight into the non-Ising character of polar domain walls by combining the SHG polarimetry analysis with modeling.

© 2021 Author(s). All article content, except where otherwise noted, is licensed under a Creative Commons Attribution (CC BY) license (<http://creativecommons.org/licenses/by/4.0/>). <https://doi.org/10.1063/5.0037286>

I. INTRODUCTION

Topological structures¹ including domain walls (DW), vortices, Bloch points, Bloch lines, bubbles, or skyrmions have attracted great attention owing to their ability to be easily created and controlled in ordered materials. When nanoscale topological structures develop in ferroic materials such as ferromagnetic, ferroelectric, or ferroelastic systems, they may represent a great playground for novel functional device concepts.^{2–4} Applications based on magnetic DWs and skyrmions have been incrementally developed by the magnetism community over the past 20 years,^{5–7} whereas the interest in topological and chiral structures in multiferroics^{2,8} and ferroelectric systems^{9–12} is comparatively new, as highlighted in recent review articles.^{13,14} Only recently, for example, ferroelectric skyrmionic structures have been predicted to exist,^{15–17} and their first observation was reported in ferroelectric/dielectric heterostructures.¹⁸ These newly discovered aspects are expected to pave the way toward applications, similar to

the developments achieved in magnetism, which further motivates an intensified research in this field.

In this context, fundamental researchers and technology developers have joined forces to explore DWs.¹⁹ An early thermodynamic study reported by Lajzerowicz and Niez²⁰ predicted the existence of a phase transition within ferroelectric DWs, while the adjacent domains remain unchanged. This has laid the foundation for the discovery of unusual polar internal structures at DWs with non-Ising^{21–24} internal structures, which are often predicted to show chiral^{25–27} or bichiral^{28,29} configurations. Nowadays, DWs are regarded as individual functional topological structures^{30–32} presenting physical properties that can be fundamentally different from those of the material in which they develop. They can be polar in non-polar materials,^{33,34} show conductivity^{35–44} or even superconductivity⁴⁵ in otherwise insulating materials, and present mechanical properties different from those of the adjacent domains.⁴⁶

These fascinating properties of polar DWs have inspired the design of original electronic device concepts and solid-state memories in which ferroelectric DWs are key elements.^{31,47} Next-generation DW-based technology is being developed after the concept of DW nanoelectronics was settled in the last decade.⁴⁸ This comprises DW memristors,⁴⁹ field effect transistors,⁵⁰ multi-level non-volatile memory cells,^{51,52} and DW-based nano-diodes.⁵³ Original approaches consisting of DW-based networks are also anticipated, laying the basis for atomic-scale electronics.⁵⁴ The emergence of a polar state at twin boundaries in SrTiO₃^{55,56} has inspired the design of an original memory device based on the wall chirality.⁵⁷ In a recent review article, Ekhard Salje explains that multifunctionality can be achieved in ferroelastic materials through a smart combination of the intrinsic functionality of polar twins with the physical processes emerging from their dynamics.⁵⁸

The genuine nanoscopic scale of polar DWs, which are only a few atomic cells wide, makes their observation and study extremely challenging. Owing to its atomic resolution, transmission electron microscopy (TEM) has emerged as the method of choice for the observation of DWs.^{59–62} Nonetheless, this technique can hardly be applied in a routine manner since the sample preparation for TEM measurements is in general difficult and invasive. For instance, the interaction of the sample with the intense electron beam may alter the domain structure.⁶³ Scanning probe microscopy methods can, to some extent, present excellent alternatives through piezoresponse force microscopy (PFM) and conductive atomic force microscopy (C-AFM).⁶⁴ While C-AFM has been proven to be highly suited for probing the local conduction at DWs, PFM measurements can hardly distinguish between an internal polarization structure of the DW and an electromechanical response arising from its displacement or deformation.⁶⁵ Non-contact methods in which specimen–probe interactions are reduced should therefore be preferred for the study of the internal structure of DWs. Polarized soft x-ray photoemission electron microscopy combined with low energy electron microscopy allows for the non-invasive study of domain structures in ferroic materials with a lateral resolution better than 50 nm,⁶⁶ which is sufficient to map the local electrostatic potential at the domain boundary regions.^{67–69} Nevertheless, this method probes only the topmost surface, and it requires a thorough surface treatment in ultrahigh vacuum conditions prior to the measurements in order to reduce surface contamination and external charge screening which strongly affects the quality of the detected signal. In contrast to this, in optical studies, the experiments are usually conducted in an ambient atmosphere and no substantial sample preparation is required. Although optical methods have long been shunned because of their limited lateral resolution, they have made it possible to evidence important properties such as DWs birefringence⁷⁰ and three-dimensional (3D) polarization structures,⁷¹ accumulation of defects,^{72,73} as well as local strain, electric fields, and unusual internal structures.⁷⁴ The modern literature on this topic includes several articles and text books discussing optical studies on domains and DWs, like the recent review by Nataf and Guennou,⁷⁵ a book chapter on three-dimensional optical studies of ferroelectric DWs,⁷⁶ as well as different articles addressing the complementarity between scanning probe microscopy, spectro-microscopy, and optical methods.^{77–79}

Non-linear optical methods have emerged as powerful, user-friendly, and non-invasive means to study polar nano- and

microstructures showing time or space inversion symmetry breaking, through a frequency doubling process known as second-harmonic generation (SHG).⁸⁰ When the non-linear optical signal is collected by means of near field, wide field, or far field microscopes, spatial distribution of the SHG can be accessed. This provides the possibility to probe ferroic domains in magnetic,^{81,82} ferroelectric,^{83,84} and complex multiferroic systems.^{85–87} Recent advances on SHG studies in oxide thin films⁸⁸ involve *operando* measurements of functioning devices⁸⁹ as well as *in situ* experiments in which the domain structure can be precisely controlled during the film growth.⁹⁰ Remarkably, SHG microscopy allows for the imaging of small objects with sizes far below the optical diffraction limit, thereby making it possible to observe not only domains but also domain boundary regions.^{91–98} Recently, SHG microscopy with polarimetry analysis has been employed for the direct observation of polar twin boundaries in non-polar centrosymmetric materials.^{99–102} The method has furthermore been used to demonstrate the existence of Néel-type domain walls in PbZrTiO₃ thin films,^{23,24} and to observe chiral Bloch walls and Bloch lines, a particular type of ferroelectric topological structures, in LiTaO₃.²⁴

This Tutorial highlights the capabilities of SHG microscopy to probe polar DWs and their internal structure. It aims at providing the necessary guidance to explore ferroelectric DWs with a Bloch or Néel-type configuration. After an overview of fundamental aspects related to the local symmetry, the non-Ising character, and the properties of DWs, we present the basics of the SHG method and emphasize its ability to probe the local symmetry down to the nanoscale. We explain how insight into the non-Ising character of polar DWs can be obtained by combining SHG polarimetry analysis and modeling. A general method is presented to investigate the internal structure of DWs with arbitrary orientation. To conclude, we discuss the validity of the presented method and review the still unsettled questions regarding non-Ising DWs.

II. THE INTERNAL STRUCTURE OF POLAR DOMAIN WALLS IN FERROIC SYSTEMS

Ferroc systems,¹⁰³ such as magnetic, ferroelectric, or ferroelastic materials, are crystalline solids characterized by the existence of an order parameter inherent to the material.¹⁰⁴ In the case of ferroelectrics this is the polarization, a vectorial quantity whose magnitude at zero external fields is a material-specific constant. Although more formal definitions of the polarization can be used,¹⁰⁵ in the case of a system of finite size we can simply think of it as the density of dipole moments, described by a vector field.¹⁰⁶ The thermodynamic potential of a ferroic material, its free energy, depends on the structure of the order parameter, i.e., on the spatial distribution of the vector field. The order parameter can be manipulated with externally applied fields and it typically possesses hysteretic properties such that the distribution of the vector field is not a unique function of the externally applied field. Rather, in equilibrium, the order parameter can adopt a variety of complex structures minimizing the energy. In particular, one usually observes a spontaneous subdivision into domains, i.e., regions within the crystal in which the orientation of the order parameter is homogeneous. The orientation of the polarization changes from one domain to another. The shape and size of the domains are often irregular. On

a larger length scale, however, the ensemble of domains can display some kind of order in terms of size, orientation, and shape. The existence of domains was first postulated by Weiss¹⁰⁷ in ferromagnetic materials and it was thereafter evidenced in ferroelectric and ferroelastic systems.^{108,109} Domains are typically very large compared to the atomic lattice constant, but smaller than the sample size (else the sample is said to be in a single-domain state). The size of domains is also much larger than that of the regions separating them, where the order parameter undergoes a transition from one orientation to another. Those transition regions between the domains are the DWs, which are at the core of this Tutorial.

The quest for miniaturization in modern nanotechnology has motivated scientists to focus their research on ferroic systems with reduced dimensionalities such as thin films and nanostructures. In this context, the importance of domains and DWs have tremendously increased in virtue of the Landau–Lifshitz–Kittel law^{110,111} that lays the theoretical basics for the formation of domains (stripe and closure domains) and demonstrates the variation of their density (or size) with the thickness. It shows, in particular, a larger domain density in very thin films and a growth of the domain size with the square root of the film thickness. Soon after its derivation for magnetic systems, the Landau–Lifshitz–Kittel law has been extended to ferroelectric domains and DWs.¹⁰⁸ More recently, this law has been updated and modernized.^{112,113} A thorough discussion on domains in ferroic crystals and thin films can be found in the book by Tagantsev *et al.*,¹¹⁴ as well as in various articles on nano- and microdomain engineering.^{115–117}

In the following, we briefly discuss the analytic form of one-dimensional profiles describing the transition between two neighboring domains with opposite polarization such that the polarization changes its direction by 180° within the DW.

A. Ising-type 180° domain walls

The theoretical analysis of the profile of domain walls in ferroelectrics is based on the energy terms dominating the structure of the polarization in the material, combined with boundary conditions enforcing the formation of the structures. In a single-component representation, the Gibbs free energy density of a ferroelectric material can be written in terms of even powers of the order parameter P_z ,¹⁰⁶

$$\Phi(P_z) = \Phi_0 + \frac{1}{2}\alpha P_z^2 + \frac{1}{4}\beta P_z^4. \quad (1)$$

The Gibbs energy is a function of the electric field E and the strain σ . From the equation of state it follows that, at constant strain σ , the changes in the energy caused by an electric field are

$$\left(\frac{\partial\Phi}{\partial P}\right)_\sigma = E \quad (2)$$

and hence,

$$E = P(\alpha + \beta P^2). \quad (3)$$

The solution describing a spontaneous, i.e., non-zero polarization P_0 at $E = 0$ is given by

$$\alpha = -\beta P_0^2. \quad (4)$$

The representation of the thermodynamic potential according to Eq. (1) describes the properties of a homogeneous ferroelectric material. In the case of spatially varying polarization structures, $P_z = P_z(x)$, a further term is required in order to account for the additional energy related to these inhomogeneities. Because changes in the polarization are usually related to a change in the crystal structure, inhomogeneous structures of the polarization are generally accompanied by a local strain that increases the energy of the system. As a result, ferroelectric materials have a tendency to preserve a homogeneous polarization structure. Regardless of its microscopic origin, this tendency can be captured in a phenomenological approach by including gradient terms of the energy term, which penalizes any inhomogeneity of the polarization. Such an approach is also well known in the case of ferromagnets, where the exchange energy tends to prevent inhomogeneities of the magnetization structure. An energy term combining various spatial derivatives of the magnetization is obtained with coefficients that must be compatible with certain symmetry properties.¹¹⁸ In ferroelectrics, a similar gradient term in the energy is known as the *correlation energy*. Using a single-component representation of P , this inhomogeneity energy density can be written as follows:

$$e_{inhom} = \gamma \left(\frac{\partial P_z}{\partial x}\right)^2. \quad (5)$$

In the one-dimensional case of a 180° domain wall, the polarization changes sign in the transition from one domain to the other. This transition leads to the boundary conditions,

$$P_z(x \rightarrow -\infty) = -P_0 \text{ and } P_z(x \rightarrow \infty) = P_0. \quad (6)$$

Removing the background energy term Φ_0 that is independent of P_z , the total energy of the one-dimensional system is

$$U = \int_{-\infty}^{\infty} \left[\frac{1}{2}\alpha P_z^2 + \frac{1}{4}\beta P_z^4 + \gamma P_0 \left(\frac{\partial P_z}{\partial x}\right)^2 \right] dx. \quad (7)$$

We seek the domain wall profile $P_z(x)$ which minimizes Eq. (7) under the conditions (6). The Euler–Lagrange equation of the energy functional can be used to derive this profile,

$$\frac{d}{dx} \left(\frac{\partial \Phi}{\partial \left(\frac{\partial P_z}{\partial x}\right)} \right) - \frac{\partial \Phi}{\partial P_z} = 0, \quad (8)$$

which yields

$$\gamma \frac{\partial^2 P_z}{\partial x^2} = \alpha P_z \left(1 - \frac{P_z^2}{P_0^2} \right). \quad (9)$$

This equation has a kink-type solution¹¹⁹

$$P_z(x) = P_0 \tanh\left(\frac{x}{\lambda}\right) \quad (10)$$

that fulfills the boundary conditions (6).

The parameter,

$$\lambda = \sqrt{-2\gamma/\alpha}, \quad (11)$$

represents the scale of x in Eq. (10), and it is, thus, a measure for the width of the domain wall. Since domain walls form a *continuous* transition between two domains, the definition of their width is not unique. The commonly used definition of the width w is

$$w = 2\lambda = \sqrt{\frac{-8\gamma}{\alpha}}. \quad (12)$$

This definition of the domain wall width can be interpreted as the distance between the intersection points of the slope of the polarization profile at the center of the domain wall with the asymptotically approached value of the polarization in the domains, as shown in Fig. 1.

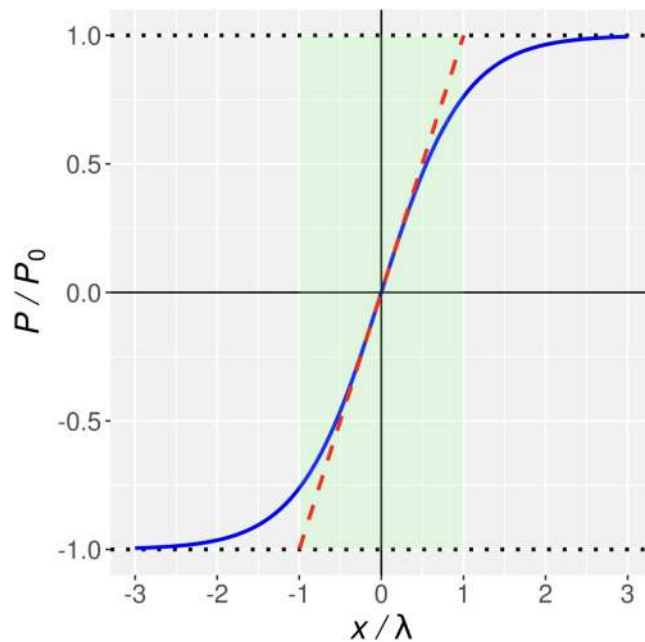


FIG. 1. Profile of an ideal one-dimensional domain wall centered at $x=0$. The position is measured in units of the domain wall parameter λ . The width of the area shaded in green defines the domain wall width w .

The DW described by Eq. (10) is known as Ising-type 180° DW. It is characterized by a single component of the polarization, which changes sign along the transition from one domain to the other through a gradual change of P_z , as shown in Fig. 1. In Sec. III, we will discuss other DW types, which involve changes in more than one polarization component. These other types of DWs correspond to those forming in ferromagnets. Although the Ising-type DW profile discussed here has been derived by using the specific energy density of a ferroelectric material, the “kink”-type transition in the form of a tanh-type profile is a general solution that is found also in other types of one-dimensional DWs, whose formation is dominated by other energy types.

B. Characteristic length scales

Beyond its specific interpretation as a domain wall width parameter, λ can more generally be regarded as a characteristic length scale on which inhomogeneities of the polarization develop within a ferroelectric material. The role of a length scale can equivalently be assigned to the correlation radius, defined as $r_c = \lambda/2$.¹¹⁴ This interpretation of the parameter λ is analogous to the role played by the *exchange lengths* in micromagnetism.¹²⁰ The magnetic exchange lengths, too, are derived from the calculation of one-dimensional domain wall profiles, and they are used to describe more generally the characteristic size of inhomogeneous magnetization structures, such as vortices or more complicated three-dimensional domain wall types. Exchange lengths also play an important practical role in simulation studies, where they represent estimates for the required size of the discretization cells used in numerical calculations. Within the framework of Landau’s theory, the correlation length λ in ferroelectrics depends sensitively on the temperature due to $\alpha = \alpha_0/(T - T_0)$, where T_0 is the Curie temperature. This dependence of the domain wall width on the temperature in ferroelectrics is different from the situation in ferromagnets, where exchange lengths are usually considered to be material-specific parameters that are not significantly affected by external parameters.

It is worth pointing out that the value of λ , and hence the width of the domain wall, is determined by the outcome of competing interactions. As discussed before, the energy term proportional to γ , the correlation energy, tends to avoid inhomogeneities of the polarization. Therefore, if a change of sign has to occur between two domains, then this term favors a transition on a scale that is as large as possible such that the gradient of P remains small. In contrast to this, the other terms in Eq. (7) which are proportional to P_z^2 favor maximization of $|P_z|$ at temperatures below T_0 . If the boundary conditions impose a change $-P_0 \rightarrow P_0$ between the domains, then these “anisotropy” terms would be minimized by shrinking the transition region as far as possible. If a spatial variation of P by 180° is enforced by the boundary conditions, then the resulting DW profile represents a compromise between these opposite tendencies.

C. Bloch and Néel-type domain walls

For a long time, DWs in ferroelectrics were believed to be exclusive of Ising type. In this ideal configuration, the polarization

decreases to zero at the DW core, and it reverses its direction while remaining parallel to the polarization of the adjacent domains (i.e., without rotation in the transition region). On the other hand, several theoretical studies have predicted the existence of polar DWs showing a clear polarization rotation^{21,25–27,29,121–128} with a non-zero planar component parallel to the DW (Bloch type) or perpendicular to it (Néel-type). These predictions were followed by experimental studies, which have confirmed the existence of non-Ising type DWs in ferroelectrics. These non-Ising DWs were named by Lee *et al.*¹²⁵ according to the corresponding fundamental types of magnetic DWs. Studies on polar DWs are currently a very active topic of research.¹⁹ In most cases, it can be assumed that non-Ising type DWs are not “pure” Bloch or Néel, but rather a mixed form of DW types combining, e.g., the characteristics of a Bloch wall and an Ising wall.¹²⁵

A fair amount of knowledge on ferroelectric DWs is based on the comparison with the well-established concepts of ferromagnetic DWs. In this context, it is useful to emphasize the differences and commonalities between the domains forming in these ferroic materials. Compared to ferroelectric domain walls, the mathematical description of magnetic domain walls has an additional complication related to the presence of a non-linear constraint: the magnetization can only change its direction not its magnitude. Therefore, unlike the polarization in Ising walls, the value of the magnetization cannot drop to zero in the center of a magnetic domain wall. Instead, it must rotate by 180° along with the transition from one domain to the other. There are two fundamental one-dimensional 180° DW types in ferromagnetism, which differ by the plane in which the magnetization rotates as it changes direction: the Bloch wall and the Néel wall. In the following, we describe these domain profiles in the case of a transition of the polarization $\mathbf{P}(x)$ in a ferroelectric material in the same way as a magnetic domain wall profile $\mathbf{M}(x)$ in a ferromagnet, even though the vector field \mathbf{P} is not subject to the same constraints as \mathbf{M} .

The Bloch wall is characterized by a rotation of the order parameter around the normal of the domain wall. Like in the Ising wall, the spatial dependence of the z component is described by a

“kink”-type profile, proportional to $\tanh(x/\lambda_B)$, but in the case of the Bloch wall, the y component also changes in the transition region, such as to preserve the norm of the local polarization vector $\mathbf{P}(x)$. Since the energy of the system does not depend on the sense of rotation of \mathbf{P} with respect to the domain wall normal, the Bloch wall can appear in two different flavors with different handedness. The Bloch wall is, thus, a chiral domain wall type.

In the case of the Néel wall, the rotation of the order parameter occurs on a plane that is perpendicular to the domain wall, leading to a non-zero x component in the domain wall region. The kink-type profile of the z component proportional to $\tanh(x/\lambda_N)$ is found also in this case. In Néel walls, the rotation can also occur in two equivalent and opposite directions, resulting in two variants with opposite signs of the x component. In nominally neutral 180° DWs, the Bloch wall transition does not contain divergences ($\nabla \cdot \mathbf{P} = 0$), and, therefore, this wall type is said to be uncharged. This is in contrast to the Néel wall, which generates regions of opposite bound charge density $\rho_b = -\nabla \cdot \mathbf{P}$ near the center of the domain wall.

Idealized profiles of an Ising wall, a Bloch wall, and a Néel wall are displayed in the bottom row of Fig. 2. In spite of the similarities in the shape of their profile, the three domain wall types generally have different widths since their respective DW parameters λ_N , λ_I , and λ_B have different functional forms. In magnetism, the parameters λ_B and λ_N are related to two different types of exchange lengths. It is obvious that the three domain wall types shown in Fig. 2 have different symmetry properties. Each of these DWs has local symmetry properties that are not only different from those of the other DW types but also from those of the parent material within the domains. As will be discussed in detail in Sec. III C, this fact can be exploited by experimental techniques that are particularly sensitive to changes in the local symmetry to both detect the DWs and to obtain indirect information on the internal structure of the polarization within the walls. In particular, this can be achieved with optical investigations based on SHG. Even though the DWs are too small to be resolved directly by such optical methods, their presence leads to characteristic

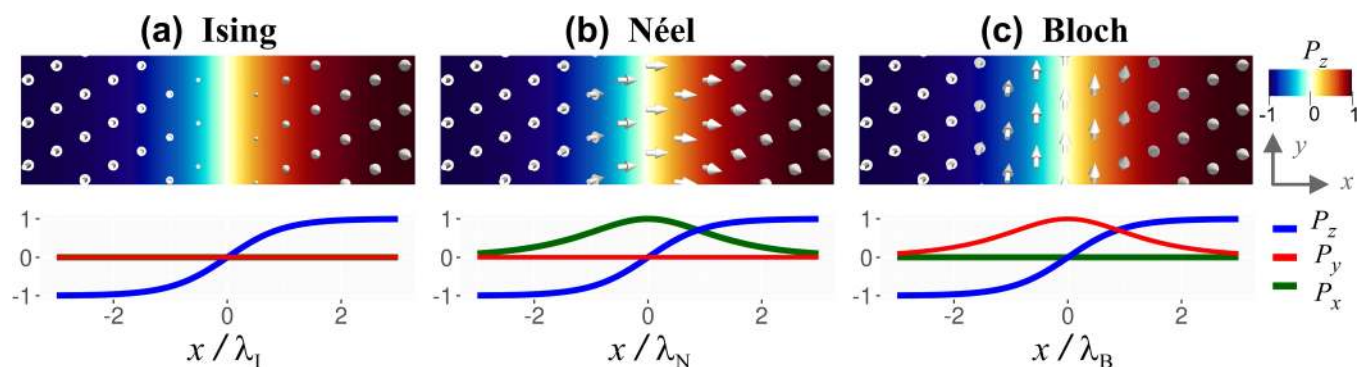


FIG. 2. Comparison of the three fundamental 180° domain wall types: (a) Ising, (b) Néel, and (c) Bloch. The arrows represent the polarization vector. In all cases, the transition of the P_z component occurs through a typical kink-type profile (blue curves). While the Ising wall is characterized by a change of the P_z component only, the Bloch domain wall and the Néel-type domain describe a rotation of the polarization, which also involves changes of the P_y and the P_x components, respectively.

changes in the local symmetry which can be detected and analyzed by SHG polarimetry.

III. FUNDAMENTAL ASPECTS OF NON-LINEAR OPTICS

Non-linear optics refers to the field of research studying the interaction of light with matter in the regime where the response of the material to the applied electromagnetic wave is non-linear. In this regime, the light-matter interaction can induce optical fields (i.e., a light emission) at frequencies (or wavelengths) different from those with which the material is irradiated, corresponding to harmonics of the incident wave. The principles of the optical harmonic generation process have long been known. The process was already anticipated in the 1930s with the theoretical work conducted by Maria Goeppert Mayer¹²⁹ during her Ph.D. However, the low-power light sources available at that time did not allow for the experimental demonstration of this effect. The era of modern non-linear optics came after the invention of powerful light sources in the form of lasers (intense and coherent light sources) and the experimental evidence of the second-harmonic generation process by Frankel *et al.*⁸⁰ Non-linear optics has since become an important field of research with high impact on the photonics industry, where such processes are exploited for frequency conversion and power amplification. Extensive information on the basic principles of non-linear optics can be found in history books published in the mid-1960s^{130,131} as well as in the recent literature.^{132,133}

In the following, after introducing fundamental aspects of the frequency doubling process, we provide a hands-on method to determine the internal structure of polar DWs based on SHG polarimetry measurements (i.e., experiments recording the variation of the SHG intensity as a function of the laser polarization and analyzer angle). We first derive the analytic form of the SHG and its dependence on light polarization. This will include a detailed description of the non-linear optical susceptibility tensor, which is a key element in the SHG process. The modeling of the SHG polarimetry response is then obtained by assuming the symmetry of the parent material, the local symmetry reduction at the DWs, and their non-Ising character (i.e., Bloch or Néel-type transitions). The validity of the model is finally assessed by fitting the experimental data with the as-derived analytic form of SHG. Note that, for didactic reasons, the modeling of the SHG signal presented in this Tutorial is simplified. A more detailed description of advanced numerical modeling of SHG microscopy and polarimetry can be found in the specialized literature (see, e.g., Ref. 134 and references therein). In particular, detailed information on field distributions in strongly focused laser beams can be found in the text books by Gu¹³⁵ or Novotny and Hecht.¹³⁶ Furthermore, optical effects related to phase shift and birefringence^{137,138} or to the light depolarization induced by a strong focusing of the incident laser beam in polarized laser microscopy have been discussed by different authors.^{139–141} Some of these aspects can be implemented in the model, depending on the measurement geometry and the complexity of the studied system. For instance, Spychala *et al.*¹⁴² have recently used vectorial modeling of the second-harmonic emission at DWs to account for the effect of strong field focusing occurring when objective lenses with particularly large numerical apertures (0.95) are used.

A. Second-harmonic generation: A frequency doubling process

Light traveling through a dielectric material at a given frequency induces, at the atomic level, a charge separation creating local electric dipoles, i.e., a rapidly varying polarization \mathbf{P} , that is proportional to the electric field \mathbf{E} of the incoming wave. At low intensities, the induced polarization is linearly proportional to the oscillating electric field of the incident beam, and the radiating dipoles produce an outgoing beam at the same frequency. However, at high incident intensities, the oscillations of the induced dipoles do not follow the frequency of the incoming wave, and different frequency components can be contained in the radiated wave. The optical response of the material can be accounted for by expanding the polarization in a power series of the incident electric field,

$$P_i = \epsilon_0 \sum_j \chi_{ij}^{(1)} E_j + \epsilon_0 \sum_{j,k,\dots} (D^{(2)} \chi_{ijk}^{(2)} E_j E_k + D^{(3)} \chi_{ijkl}^{(3)} E_j E_k E_l + \dots). \quad (13)$$

The first term in Eq. (13) represents the linear polarization and the higher-order terms correspond to the non-linear polarization response. ϵ_0 is the vacuum permittivity, D is a degeneracy factor, $\chi^{(m)}$ is the m th order optical susceptibility tensor, and the indices i, j, k refer to the Cartesian laboratory coordinates (x, y, z) . The second term represents the second-harmonic generation process occurring in non-centrosymmetric materials such as ferroelectrics. In a microscopic picture, it involves the coupling of two incident photons at frequency ω that produce a polarization oscillating with the double frequency $P(2\omega)$,

$$P_l(2\omega) = \epsilon_0 D^{(2)} \chi_{lmn}^{(2)} E_m(\omega) E_n(\omega). \quad (14)$$

This non-linear process arises in non-centrosymmetric crystals in which the second-order non-linear optical susceptibility $\chi^{(2)}$ is non-zero. The intrinsic permutation symmetry allows the susceptibility tensor to be replaced by a contracted d -tensor following the Voigt notation: $2d_{ij} = \chi_{ikl}^{(2)}$. The degeneracy factor is $D^{(2)} = 1/2$ for indistinguishable fields involved in SHG and optical rectification. The number of the non-vanishing d_{ij} elements is further reduced when considering the point group symmetry of the material according to Neumann's principle. The SHG intensity is given by $I^{SHG} = |P(2\omega)|^2 = \sum_i (P_i(2\omega))^2$, where

$$\begin{pmatrix} P_x(2\omega) \\ P_y(2\omega) \\ P_z(2\omega) \end{pmatrix} = \epsilon_0 \begin{pmatrix} d_{11} & d_{12} & d_{13} & d_{14} & d_{15} & d_{16} \\ d_{21} & d_{22} & d_{23} & d_{24} & d_{25} & d_{26} \\ d_{31} & d_{32} & d_{33} & d_{34} & d_{35} & d_{36} \end{pmatrix} \times \begin{pmatrix} E_x^2(\omega) \\ E_y^2(\omega) \\ E_z^2(\omega) \\ 2 E_y(\omega) E_z(\omega) \\ 2 E_x(\omega) E_z(\omega) \\ 2 E_x(\omega) E_y(\omega) \end{pmatrix}. \quad (15)$$

The intensity of the second-harmonic emission varies quadratically with the power of the incident laser, in addition to the

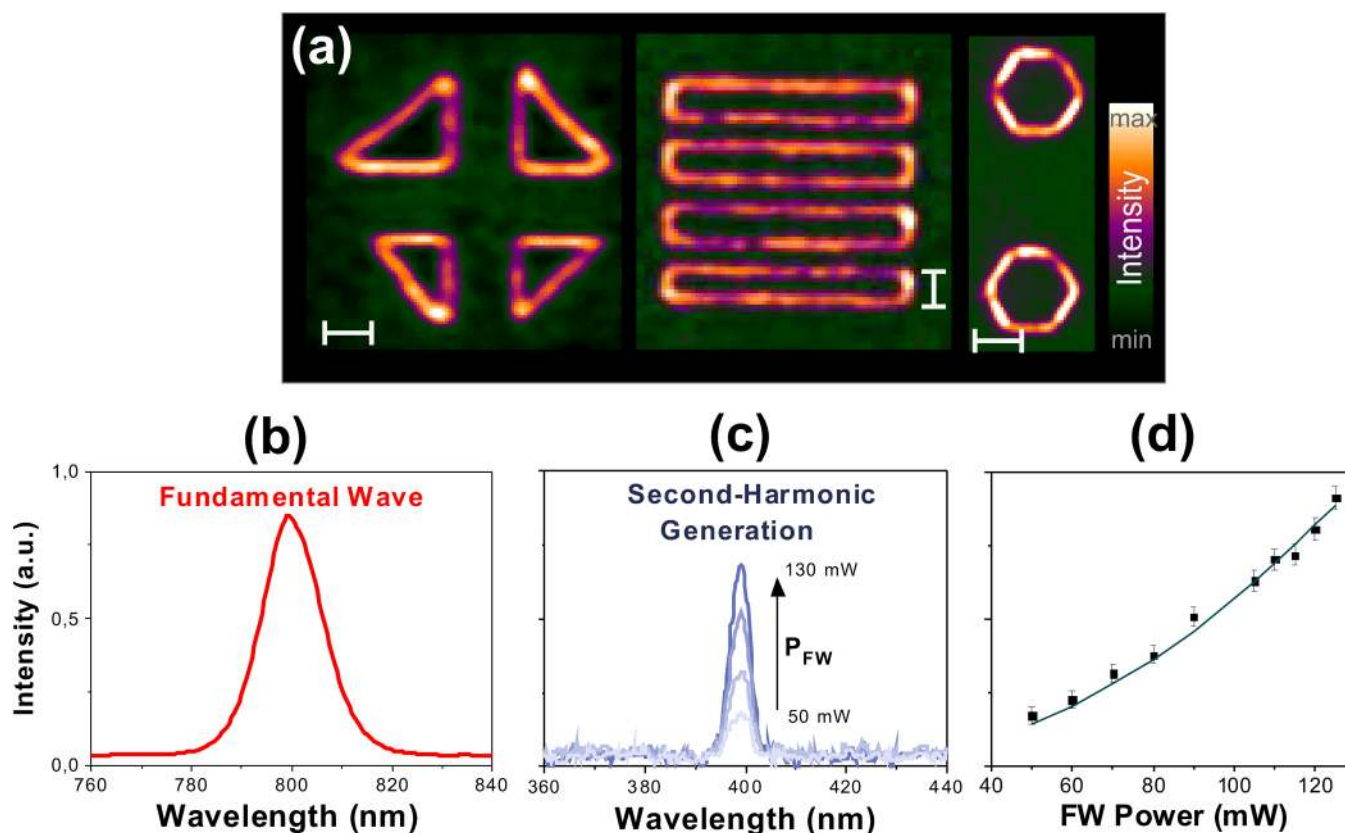


FIG. 3. Evidence of a frequency doubling process at ferroelectric domain walls. (a) A localized emission is evidenced at 180° walls in PbZrTiO_3 thin films (triangular and rectangular shape domains) and in LiTaO_3 (hexagonal shape domains). The bars in the images displayed in panel (a) correspond to a scale of $2\ \mu\text{m}$ for the triangles and rectangles and $15\ \mu\text{m}$ in the hexagon. The spectral analysis of this DW emission shows that while (b) the fundamental wave (FW) is 800 nm, the (c) emitted wavelength (400 nm) corresponds to half of the fundamental wavelength. (d) The intensity of the localized DW emission increases quadratically with the power of the FW. Adapted from Cherifi-Hertel *et al.*, Nat. Commun. **8**, 15768 (2017). Copyright 2017 Authors, licensed under a Creative Commons Attribution (CC BY 4.0) license.

frequency doubling process. Therefore, non-linear materials, which allow for both signal amplification and efficient energy transfer from one wave to another, are key elements in the photonic industry. Figure 3 shows that ferroelectric domains imaged in an SHG microscope exhibit a localized emission at the DWs. The intensity at the DWs is found to increase quadratically with the laser power [Fig. 3(d)] and the emission wavelength corresponds to half of the fundamental wavelength (i.e., the double of the frequency). This is an unambiguous signature of SHG. Such spectral analysis can be easily implemented in standard optical microscopes in which the operative mode can be switched from spectroscopy to imaging by means of a movable mirror. Note that, in principle, photon counting allows for quantitative analysis of the SHG intensity. This is however a delicate task since it requires a rigorous comparative study with a reference sample. Moreover, the SHG intensity can depend on the sample form (bulk or the thin film) and on the detection geometry involving forward, backward, or reflected backward SHG signals.¹⁴³ We present in the following the SHG intensity in arbitrary units and

use the polarimetry analysis to obtain the internal polar structure of the DWs (i.e., the orientation of the polarization) rather than quantitative information on their optical properties.

B. The second-order non-linear susceptibility tensor

The susceptibility tensor in SHG is a third-rank tensor connecting a cause given by a product of a vector (a second-order term that essentially represents the square of the electric field of the incident wave) to an effect represented by a vector (the induced polarization of the material). It is an optical property of the material that reflects its structural symmetry. This comprises not only the point group symmetry of the crystal but also information about the ferroic order. In multidomain ferroelectric materials, the SHG polarimetry response depends on the crystal symmetry (which determines the non-zero d_{ij} tensor elements), the orientation of the domains (crystal coordinate system), and the measurement geometry (laboratory frame). The modeling of the optical response requires, therefore, the transformation of either the susceptibility tensor to the

laboratory system or the electric field vector to the crystal coordinates system. Although these two methods are perfectly equivalent (see, e.g., Denev *et al.*⁸³), we choose the first method for its simplicity. It requires only the knowledge of a reference susceptibility tensor d^0 defined in the crystallographic reference frame (X, Y, Z) . Any “new” tensor element corresponding to an arbitrary coordinate system (X', Y', Z') with a particular ferroelectric polarization of the underlying material can be deduced from the general rotation matrix transformations as follows:

$$d_{ij}^{New} = A_{ij} d_{kl}^0 \alpha_{ij}^{-1}, \quad (16)$$

where A is the rotation matrix resulting from the product of three individual rotations of Euler angles: ϕ , θ , ψ counterclockwise about

Z , X' and Z'' ,¹⁴⁴

$$A = (a_{ij}) = \begin{pmatrix} \cos\psi & \sin\psi & 0 \\ -\sin\psi & \cos\psi & 0 \\ 0 & 0 & 1 \end{pmatrix} \begin{pmatrix} 1 & 0 & 0 \\ 0 & \cos\theta & \sin\theta \\ 0 & -\sin\theta & \cos\theta \end{pmatrix} \times \begin{pmatrix} \cos\phi & \sin\phi & 0 \\ -\sin\phi & \cos\phi & 0 \\ 0 & 0 & 1 \end{pmatrix}. \quad (17)$$

The elements of the transformation matrix α^{-1} are functions of the directional cosines,

$$\alpha_{ij}^{-1} = \begin{pmatrix} a_{11}^2 & a_{21}^2 & a_{31}^2 & 2a_{21}a_{31} & 2a_{31}a_{11} & 2a_{11}a_{21} \\ a_{12}^2 & a_{22}^2 & a_{32}^2 & 2a_{22}a_{32} & 2a_{32}a_{12} & 2a_{12}a_{22} \\ a_{13}^2 & a_{23}^2 & a_{33}^2 & 2a_{23}a_{33} & 2a_{33}a_{13} & 2a_{13}a_{23} \\ a_{12}a_{13} & a_{22}a_{23} & a_{32}a_{33} & (a_{22}a_{33} + a_{32}a_{23}) & (a_{12}a_{33} + a_{32}a_{13}) & (a_{22}a_{13} + a_{12}a_{23}) \\ a_{13}a_{11} & a_{23}a_{21} & a_{33}a_{31} & (a_{21}a_{33} + a_{31}a_{23}) & (a_{31}a_{13} + a_{11}a_{33}) & (a_{11}a_{23} + a_{21}a_{13}) \\ a_{11}a_{12} & a_{21}a_{22} & a_{31}a_{32} & (a_{21}a_{32} + a_{31}a_{22}) & (a_{31}a_{12} + a_{11}a_{32}) & (a_{11}a_{22} + a_{21}a_{12}) \end{pmatrix}. \quad (18)$$

Note that the representation of the susceptibility tensor in an arbitrary coordinate system requires only the application of the rotation matrix of Eq. (17). The transformation matrix α^{-1} is only required if the result shall be presented in the laboratory coordinate system.

This method is often used to obtain information on the domain structure of ferroelectric¹⁴⁵ and complex multiferroic systems^{86,87,146} based on the SHG polarimetry analysis. A precise polarimetry analysis of the domain structure was reported by Gopalan and co-workers^{147,148} in studies on the evolution of the domain structure during phase transitions in KNbO_3 and $\text{Bi}_4\text{Ti}_3\text{O}_{12}$. This method was then improved by Mishina *et al.*¹⁴⁹ to account for both coherent and incoherent contributions in inhomogeneous films. SHG polarimetry has since become a routine method to study ferroelectric domain structures. The question of whether this approach can be used to investigate the polar structure of DWs, instead of the domains, arises naturally. As a starting point, we can consider the tensor d^0 corresponding to the symmetry of the parent material with an ideal Ising-type DW structure. Any deviation from the Ising configuration can be characterized by the rotation angles ϕ , θ , ψ leading to a new tensor d^{New} defined by Eq. (16). While this method is expected to give qualitative information on the local anisotropy and the possible existence of a non-Ising configuration (i.e., non-zero averaged polarization at the DWs), the local SHG at DWs cannot be correctly modeled based on the susceptibility tensor of the parent material (i.e., based solely on the symmetry and optical response of the adjacent domains).

This is because symmetry operations (e.g., tensor rotation used to model domains with different orientations) preserve the original symmetry of the susceptibility tensor, while a reduction of symmetry is expected at the domain boundary regions, as will be discussed in Sec. III C. Thus, deriving the local susceptibility tensor at DWs is indispensable. This is arguably the most challenging task in DW studies with SHG polarimetry.

C. Derivation of the susceptibility tensor at domain walls based on symmetry arguments

Besides being particularly suited for the study of non-centrosymmetric materials, SHG experiments with polarimetry analysis provide important information on symmetry.¹⁵⁰ According to the Neumann–Minnigerode–Curie principle,¹⁵¹ the physical properties of the object of interest, for instance, a DW, can be derived from its symmetry. It should, thus, be possible to identify the physical properties of DWs based on symmetry arguments. A local property tensor was derived by Přívratká and Janovec¹⁵² for nonferroelastic DWs by determining the symmetry of DWs using the crystallographic layer group¹⁵³ and by accounting for the symmetry of the adjacent domains. This approach has shown, e.g., that a spontaneous polarization or magnetization can be present at DWs in materials that do not display such ordering in their homogeneous form.¹⁵⁴ Alternatively, the DW symmetry can be deduced from the primary transition order parameter of the adjacent domains, and by taking into account a possible reduction of the

parent order parameter space at the domain boundary region.¹⁵⁵ Schranz *et al.*¹⁵⁶ have recently combined the analysis of the order parameter across the walls with the layer group analysis developed by Janovec to derive the local symmetry and the related properties at polar twin boundaries.

Based on Landau potential calculations describing phase transitions at DWs, Bul'bich and Gufan¹⁵⁷ have evidenced a symmetry lowering at DWs corresponding to a transition of a wall in which the order parameter varies only in magnitude (i.e., Ising wall) to a wall in which the change in magnitude is accompanied by a rotation of the order parameter (i.e., non-Ising wall). Nowadays, it has become clear that a DW holds its own symmetry and properties which usually differ from those of the adjacent domains. In this situation, the following question arises: can we probe the local symmetry of DWs using SHG polarimetry experiments combined with simulations to gain insight into their properties? Based on the recently reported SHG polarimetry studies of twins,¹⁰⁰ phase boundaries,¹⁵⁸ as well as ferroelectric DWs,^{23,159} we confirm that the internal structure of the DWs in terms of chirality and non-Ising characters²⁴ can indeed be accessed.

Polar twin boundaries in ferroelastic systems have been proven to exhibit either a 2 or m point group symmetry^{99,101,160} (except for LaAlO₃ that exhibits $3m$ symmetry¹⁰⁰). This result applies also to non-Ising type ferroelectric DWs with Néel and Bloch internal structures. Figure 4 displays the internal structure and symmetry of Bloch and Néel-type DWs located in the zy -plane. In this case, Bloch-type walls exhibit a point group symmetry 2, Néel-type walls show a point group symmetry m , while Ising-type DWs are centrosymmetric with a point group symmetry $2/m$. It is also worth noting that, even though the two non-Ising DW types appear in two variants, only the Bloch-type DW is chiral in the sense that it does not display a mirror symmetry.

In the following, the susceptibility tensor corresponding to Bloch and Néel-type ferroelectric DWs is derived assuming point group symmetry 2 or m . For the sake of simplicity, we assume an averaged polarization oriented along with the DW in

the Bloch case and perpendicular to it for Néel-type DWs instead of the hyperbolic tanh profile. The orientation of the DWs is given by the δ angle (δ is taken from the x axis in the laboratory coordinate system) and their susceptibility accounting for their non-Ising character is defined by the Euler angles as follows: $\phi = 0$, $\theta = 0$, $\psi = 90^\circ - \delta$. The resulting non-Ising DW susceptibility tensor with arbitrary orientation [defined by the δ angle taken from the x axis, where the laboratory coordinate system (x,y,z) coincides with the crystallographic axes (X,Y,Z)] takes the following form:

$$d^{N\acute{e}el} = \begin{pmatrix} \sin\delta & \cos\delta & 0 \\ -\cos\delta & \sin\delta & 0 \\ 0 & 0 & 1 \end{pmatrix} \begin{pmatrix} d_{11} & d_{12} & d_{13} & 0 & d_{15} & 0 \\ 0 & 0 & 0 & d_{24} & 0 & d_{26} \\ d_{31} & d_{32} & d_{33} & 0 & d_{35} & 0 \end{pmatrix} \times \begin{pmatrix} \sin^2\delta & \cos^2\delta & 0 & 0 & 0 & -\sin 2\delta \\ \cos^2\delta & \sin^2\delta & 0 & 0 & 0 & \sin 2\delta \\ 0 & 0 & 1 & 0 & 0 & 0 \\ 0 & 0 & 0 & \sin\delta & \cos\delta & 0 \\ 0 & 0 & 0 & -\cos\delta & \sin\delta & 0 \\ \frac{1}{2}\sin 2\delta & -\frac{1}{2}\sin 2\delta & 0 & 0 & 0 & -\cos 2\delta \end{pmatrix}, \quad (19)$$

$$d^{Bloch} = \begin{pmatrix} \sin\delta & \cos\delta & 0 \\ -\cos\delta & \sin\delta & 0 \\ 0 & 0 & 1 \end{pmatrix} \begin{pmatrix} 0 & 0 & 0 & d_{14} & 0 & d_{16} \\ d_{21} & d_{22} & d_{23} & 0 & d_{25} & 0 \\ 0 & 0 & 0 & d_{34} & 0 & d_{36} \end{pmatrix} \times \begin{pmatrix} \sin^2\delta & \cos^2\delta & 0 & 0 & 0 & -\sin 2\delta \\ \cos^2\delta & \sin^2\delta & 0 & 0 & 0 & \sin 2\delta \\ 0 & 0 & 1 & 0 & 0 & 0 \\ 0 & 0 & 0 & \sin\delta & \cos\delta & 0 \\ 0 & 0 & 0 & -\cos\delta & \sin\delta & 0 \\ \frac{1}{2}\sin 2\delta & -\frac{1}{2}\sin 2\delta & 0 & 0 & 0 & -\cos 2\delta \end{pmatrix}. \quad (20)$$

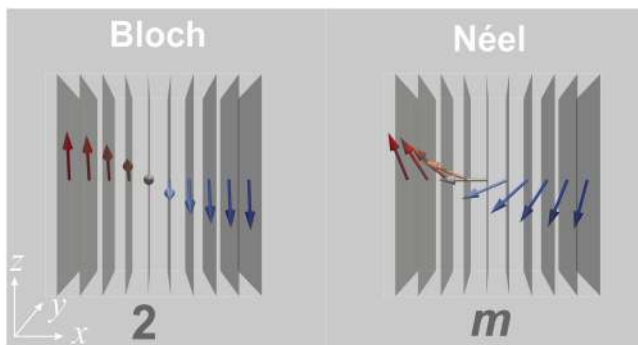


FIG. 4. Local symmetry at Bloch-type and Néel-type domain walls. Point group symmetry 2 and m are derived as discussed in the body text. The polarization rotation across the wall can be either clockwise or counterclockwise in both domain wall types.

IV. SHG MICROSCOPY AND POLARIMETRY ANALYSIS AT NON-ISING DOMAIN WALLS

A. Contrast mechanism at domain walls in SHG microscopy

The observation of ferroelectric DWs by means of SHG experiments has long been known. They can be revealed in different measurement geometries such as far field,⁹³ near field,⁹² as well as in collinear⁹¹ and noncollinear⁹⁴ (Čerenkov) SHG experiments. In these experiments, the DWs can either appear as dark lines or as bright regions. This SHG contrast variation from dark to bright results primarily from the SHG emission of the adjacent domains rather than from the measurement geometry. Fiebig *et al.*¹⁶¹ explain the dark contrast at DWs in RMnO₃ (R = Y, Ho) by destructive interference from the oppositely polarized neighboring domains. This is due to the large lateral size of the probe beam with respect to the DW, which induces an overlap of the SHG

waves emitted by the adjacent domains. Their phase shift results in destructive interference at the 180° DW, making them appear as dark lines. A local SHG emission that can be used to gain insight into the physical properties of DWs can only be observed if the emission from the domains is minimal. Therefore, SHG is particularly suited for the study of polar twin boundaries owing to the absence of SHG at the centrosymmetric neighboring domains (see Yokota *et al.*⁹⁹). In ferroelectric materials, the SHG arising from the domains may overshadow the DW signal. The orientation of the sample and the measurement geometry should be carefully chosen in this case such as to optimize the DW signal. In Sec. IV D, we will see that confocal SHG microscopy is particularly helpful in this sense, as it allows, e.g., to focus the study on the core of bulk materials where the emission from the domains is low.¹⁶²

B. Experimental details

A detailed description of all possible measurement geometries can be found in Ref. 83 and references therein. Here, we present more specifically scanning confocal microscopy in the backreflection geometry [see Fig. 5(a)] which ensures the overall non-invasive character of the method and allows for a better lateral resolution with respect to other configurations. It is furthermore particularly adapted for the study of ferroelectric thin films grown on nontransparent substrates. This type of instrument typically includes a laser source with sufficient output power to produce a non-linear response (e.g., a pulsed fs laser with 100 fs pulses and a repetition rate of 80 MHz) and a fundamental wavelength in the range of 750 nm–1000 nm. The laser beam is focused through an objective lens and directed at normal incidence to the sample, which allows

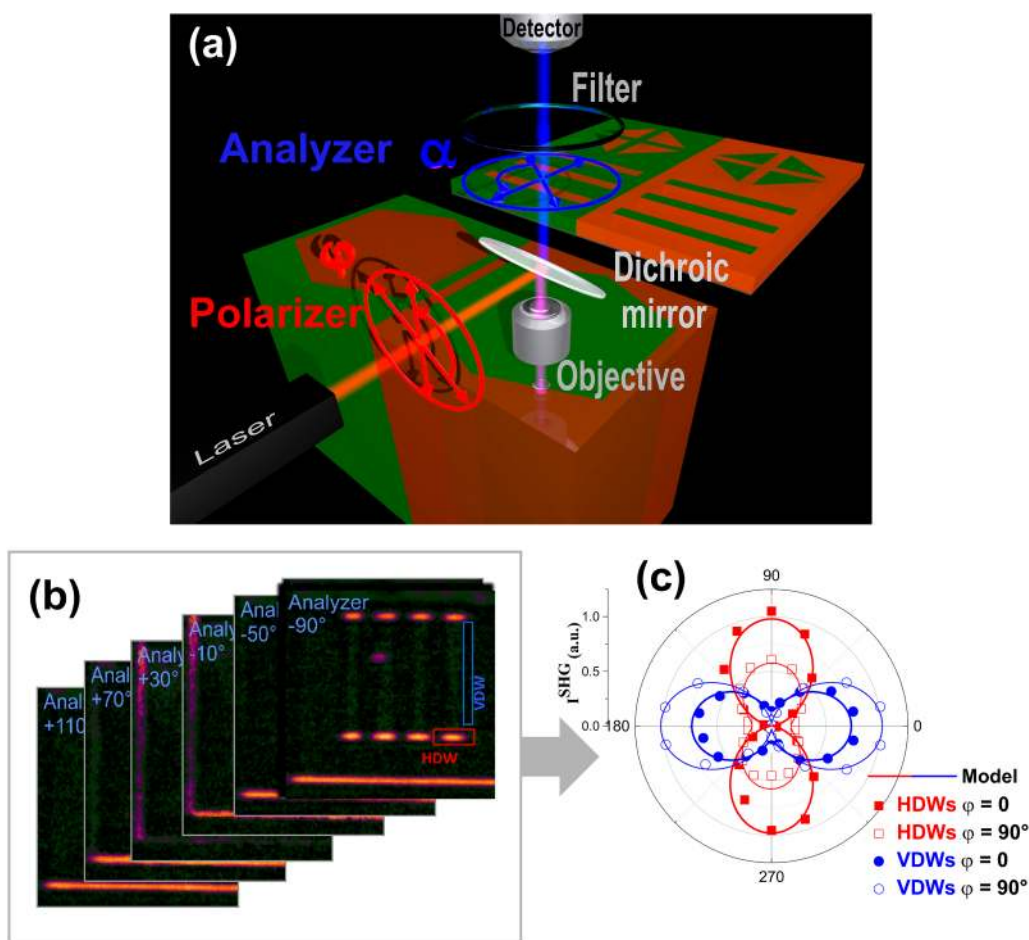


FIG. 5. (a) Schematic representation of an inverted confocal microscope in which the SHG signal is detected in reflection geometry. The focused laser beam is shined on the sample at normal incidence, and the SHG signal is collected in the collinear geometry. Polarimetry measurements are conducted using motorized linear polarizers. (b) Image series are recorded at different analyzer angles α for a given laser polarization angle ($\varphi = 0^\circ$ or 90°). The integration of the intensity over selected regions yields the local SHG variation as a function of the analyzer angle within the region of interest (red and blue boxes in the image). The result is usually displayed as a polar plot showing (c) the SHG polarimetry response at horizontal (HDW) and vertical domain walls (VDW). Adapted from Cherifi-Hertel *et al.*, Nat. Commun. 8, 15768 (2017). Copyright 2017 Authors, licensed under a Creative Commons Attribution (CC BY 4.0) license.

us to use the same objective for the imaging. The SHG images are obtained by scanning the sample with respect to the incoming beam using computer-controlled stepping motors. The output wave is spectrally filtered and transferred to a photomultiplier for imaging. When a spectral analysis of the emission signal is necessary, a mirror is inserted to deflect the emitted signal toward a spectrometer. Polarimetry measurements are performed by recording SHG images at different polarizer and analyzer angles. Objectives with high numerical apertures would normally improve the lateral resolution of the microscope. However, the use of moderate numerical apertures is recommended because the paraxial approximation is satisfied in this case. When the numerical aperture became large (e.g., in the order of 0.95 as discussed in Ref. 141), many effects such as apodization, depolarization, and aberrations can occur and must be included in the theoretical models.¹³⁵ Note that all the SHG measurements presented in this Tutorial have been obtained in the case of medium focusing (numerical aperture in the order of 0.7) for which the paraxial approximation holds.

In SHG polarimetry experiments, image series [see Fig. 5(c)] are recorded as a function of the analyzer angles α at a given laser polarization φ or vice versa (α fixed and φ rotating). The study of the SHG polarimetry anisotropy can also require measurements in which both the polarizer and analyzer are rotated (either parallel or perpendicular to each other). The integration of the intensity over a selected area of the image sequence yields the local SHG polarimetry response within the region of interest. The data are then normalized by the number of pixels of the selected region to eliminate the effect of the selected area size on the intensity. The SHG intensity variation is traditionally presented as polar plots [see Fig. 5(c)]. The fitting of the polar plots based on the analytic form of the SHG provides information on the local symmetry and polarization order.

C. Modeling the SHG polarimetry response

The SHG signal is described by the fundamental equations of the second-order non-linear process given by Eq. (15). In the measurement geometry depicted in Fig. 5(a), both the fundamental wave (FW) and the SHG emission propagate along the z axis (normal incidence), and the detection is in the reflection geometry. In this case, the electric field of the FW components lies within the (xy) plane ($E_x = E_0 \cos \varphi$, $E_y = E_0 \sin \varphi$, $E_z = 0$), where φ is the polarization angle of the FW measured from the x axis. The full SHG polarimetry response is given by

$$\begin{pmatrix} P_x^{2\omega}(\varphi) \\ P_y^{2\omega}(\varphi) \\ P_z^{2\omega}(\varphi) \end{pmatrix} = \epsilon_0 \begin{pmatrix} d_{11} & d_{12} & d_{13} & d_{14} & d_{15} & d_{16} \\ d_{21} & d_{22} & d_{23} & d_{24} & d_{25} & d_{26} \\ d_{31} & d_{32} & d_{33} & d_{34} & d_{35} & d_{36} \end{pmatrix} \begin{pmatrix} E_0^2 \cos^2 \varphi \\ E_0^2 \sin^2 \varphi \\ 0 \\ 0 \\ 0 \\ E_0^2 \sin 2\varphi \end{pmatrix}. \quad (21)$$

The polarization signal after traversing the linear output analyzer is obtained as a function of the orientation of the analyzer angle α by using the Jones formalism for a linear polarizer with a

transmission angle α ,

$$\begin{pmatrix} P_x^{2\omega}(\varphi, \alpha) \\ P_y^{2\omega}(\varphi, \alpha) \\ P_z^{2\omega}(\varphi, \alpha) \end{pmatrix} = \begin{pmatrix} \cos^2 \alpha & \cos \alpha \sin \alpha & 0 \\ \cos \alpha \sin \alpha & \sin^2 \alpha & 0 \\ 0 & 0 & 1 \end{pmatrix} \begin{pmatrix} P_x^{2\omega}(\varphi) \\ P_y^{2\omega}(\varphi) \\ P_z^{2\omega}(\varphi) \end{pmatrix}. \quad (22)$$

Equations (21) and (22) provide a complete description of the SHG polarimetry response $I^{SHG}(\varphi, \alpha) = |P^{2\omega}(\varphi, \alpha)|^2$. This general approach is adapted for the study of the internal structure of polar DWs by taking into account its specific local symmetry and assuming a Néel-type or Bloch-type internal structure, i.e., using the susceptibility tensors given by Eqs. (19) and (20). The comparison between the data obtained in the experiment and the expected data by assuming different analytic models allows us to infer the structure of the observed DWs.

Figure 6 shows a detailed SHG polarimetry analysis at DWs surrounding c -domains (i.e., domains with out-of-plane polarization pointing either upward c^+ or downward c^- on a background with opposite polarity). Two different systems are considered: tetragonal PbZrTiO_3 (point group $4mm$) thin films showing triangular shape domains and LiTaO_3 bulk crystals (point group $3m$) with hexagonal shape domains. If we focus on horizontal DWs, i.e., DWs parallel to the x axis ($\delta = 0^\circ$), we observe that the local polar plots display a maximum along with the DW in LiTaO_3 [see Fig. 6(b)], while the maximum is perpendicular to the DW in PbZrTiO_3 [see Fig. 6(d)]. This polarimetry response suggests a Néel-like character in PbZrTiO_3 and a Bloch-like response in LiTaO_3 hexagons. This result is confirmed by the simulation of the SHG polar plots at DWs with different angles [see Figs. 6(c)–6(e)] and by the good agreement of the fit of the experimental data using a Néel model PbZrTiO_3 and a Bloch model in LiTaO_3 .

In order to confirm the ability of SHG polarimetry to distinguish between Bloch-like and Néel-like characters, advanced 2D simulations of the SHG images have been conducted. In this model, the DW region is subdivided into discrete regions, in which the ferroelectric polarization is allowed to rotate. The susceptibility tensor is then calculated at each rotation angle. This allows deriving the expected SHG intensity at any position (pixel) in both the domains and DW regions for given polarizer and analyzer angles. The result is displayed in Fig. 7 for a square shape domain. The isotropic SHG image (i.e., without polarization analysis) shows localized SHG emission at non-Ising DWs, in agreement with the experiments [see, e.g., Fig. 3(a)]. Moreover, the polarimetry response (characterized by the variation of contrast in SHG images with the analyzer and polarizer angles) shows clear and distinct signatures for Néel [Fig. 3(b)] and Bloch-type [Fig. 3(c)] characters.

The existence of Néel-type ferroelectric DWs is currently debated among theoreticians and experimentalists. In fact, Néel DWs are intrinsically charged, even in nominally neutral 180° DWs, which makes them energetically less favorable than Bloch-type walls. Yet, a Néel-like configuration is more often observed in experimental studies than the Bloch type (observed so far only in nearly stoichiometric LiTaO_3 ²⁴). Tetragonal PbZrTiO_3 (often used as a stand-in system for pure PbTiO_3) has been reported to exhibit Néel-type DWs in experiments conducted at room temperature, while Bloch-type walls have been predicted in

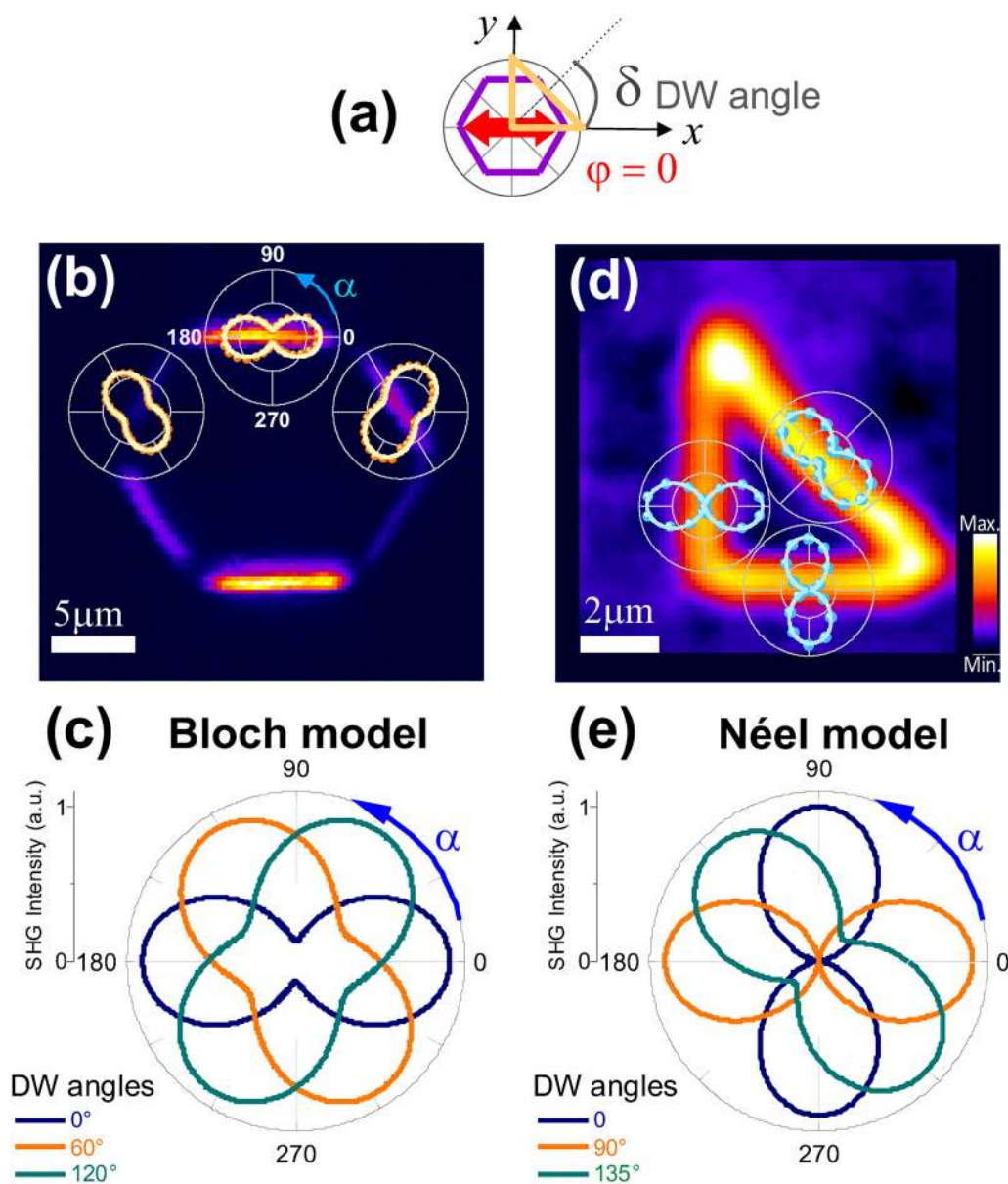


FIG. 6. Local SHG polarimetry analysis at ferroelectric DWs. Panel (a) shows a schematic representation of the SHG measurement geometry. The laser polarization (red arrow) is along the x axis, and the DW tilt angle δ is taken with respect to the x axis (the case $\delta = 0$ corresponds, e.g., to a wall along x). Isotropic SHG images are shown in the case of (b) a hexagonal shape domain in LiTaO_3 crystal, and (d) a triangular shape domain in PbZrTiO_3 thin films. The local polar plots showing the variation of the SHG intensity with the analyzer angle α are positioned on the corresponding DW. The experimental data are well fitted using Bloch model in the case of trigonal LiTaO_3 (c) and the Néel model in the case of tetragonal PbZrTiO_3 (e). Adapted from Cherifi-Hertel *et al.*, *Nat. Commun.* **8**, 15768 (2017). Copyright 2017 Authors, licensed under a Creative Commons Attribution (CC BY 4.0) license.

PbTiO_3 .^{123,163} This discrepancy between theory and experiments can be related to a difference in the temperature at which the studies are conducted. A recent work combining theory and experiments has evidenced a dependence of the polar order with the magnitude on the configurational entropy.¹⁶⁴ The increased

entropy at the DW regions was directly linked to the Néel-like component in LiNbO_3 . Two other effects may also change the internal structure of the DWs in tetragonal PbZrTiO_3 thin films: (i) the tilt angle of the walls with respect to the polar axis²³ and (ii) the 3D polar structure of the DW in the volume, which could

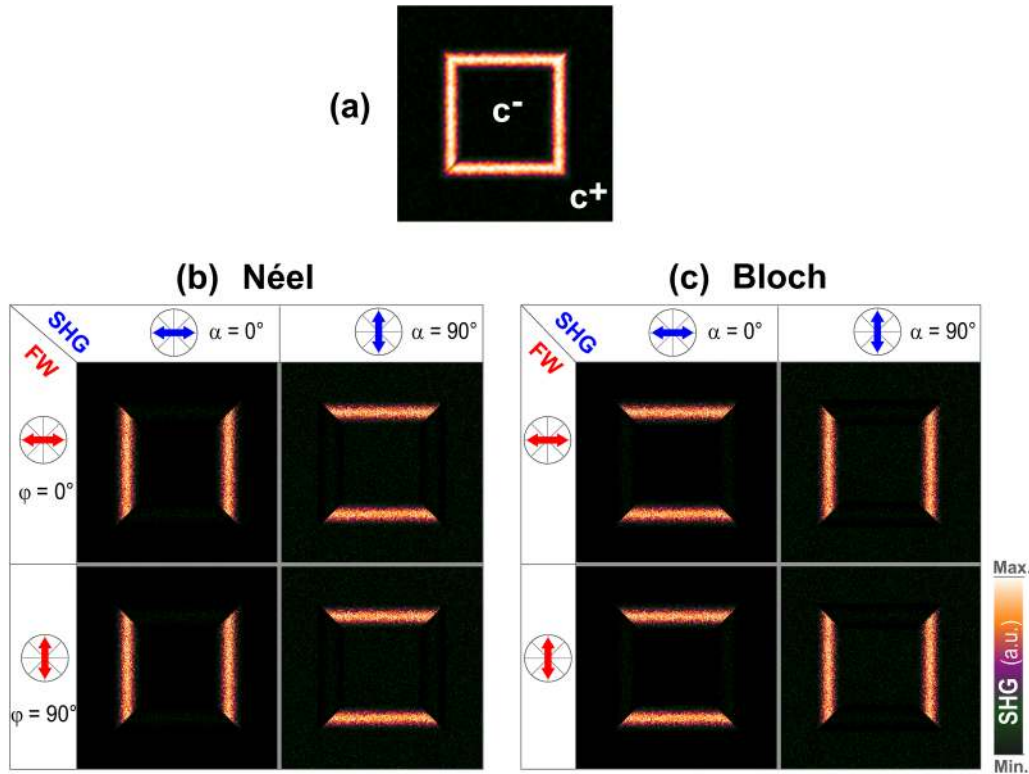


FIG. 7. Two-dimensional numerical simulations of SHG images of a square shape domain with out-of-plane polarization and 180° non-Ising type domain walls separating the c^+ and c^- domains. The isotropic SHG response in both Néel (a) and Bloch (not shown) models shows a localized SHG emission at the domain wall regions. The polarimetry response characterized by the variations of the SHG contrast at the domain walls with different polarizer (φ , red arrow) and analyzer (α , blue arrow) angles shows a complementary response between (b) Néel and (c) Bloch models. Using such comparisons, SHG microscopy with polarimetry analysis is capable of clearly distinguishing between domain walls with a Néel-type and a Bloch-type character. Adapted from Cherifi-Hertel *et al.*, Nat. Commun. 8, 15768 (2017). Copyright 2017 Authors, licensed under a Creative Commons Attribution (CC BY 4.0) license.

be Bloch- or Ising-like in the volume and of Néel-type at the topmost surface, as recently suggested by Li *et al.*¹⁶⁵

D. Three-dimensional domain wall profiles in SHG experiments

Confocal SHG microscopy is particularly adapted for the mapping of the SHG response in three dimensions.^{166,167} Both collinear (presented in this Tutorial) and non-collinear SHG known as Čerenkov SHG can be conducted for this purpose.⁷⁶ The use of galvanometric scanners to control the laser beam position in Čerenkov type SHG provides fast imaging of the DW morphology in three dimensions. This has permitted, e.g., establishing direct correlations between the 3D morphology of the walls in lithium niobate,¹⁶⁸ their charged character,^{169,170} and their enhanced conductivity. Owing to the fast acquisition of the images, this method is often applied to study DW kinetics as a function of electric¹⁷¹ or temperature¹⁷² stimuli. These temperature- or field-driven kinetic processes are known to yield exotic domain patterns¹⁷³ with closely packed charged DWs showing, e.g., zig-zag shapes. The study of the local

SHG emission in such complex systems is rather challenging since it involves interfering signals including different DWs or a domain wall and a background SHG signal resulting from the adjacent domain or interface effects as discussed by Kämpfe *et al.*¹⁷⁴ In fact, a background signal with a characteristic polarimetry response often results from the electric field discontinuity occurring at surfaces and interface^{175,176} in thin films. Even if the intensity of this surface-induced second-harmonic emission is small, the subtraction of such anisotropic background may be difficult, especially when this signal interferes with that of phase-shifted SHG nanoemitters. Optimum measurement conditions are thus obtained in the case of isolated DWs and minimum background signal.

In collinear SHG [e.g., in the measurement geometry displayed in Fig. 5(a)], the sample is usually scanned with respect to the laser beam. This makes the acquisition of the images rather slow with a typical scan rate of 100 nm/20 ms. Nevertheless, this method allows the combination of precise local polarimetry analysis with high-resolution imaging that is necessary to study topological structures such as non-Ising and chiral DWs.²⁴ Collinear SHG microscopy is optimized for 2D imaging. Yet, a 3D image can be

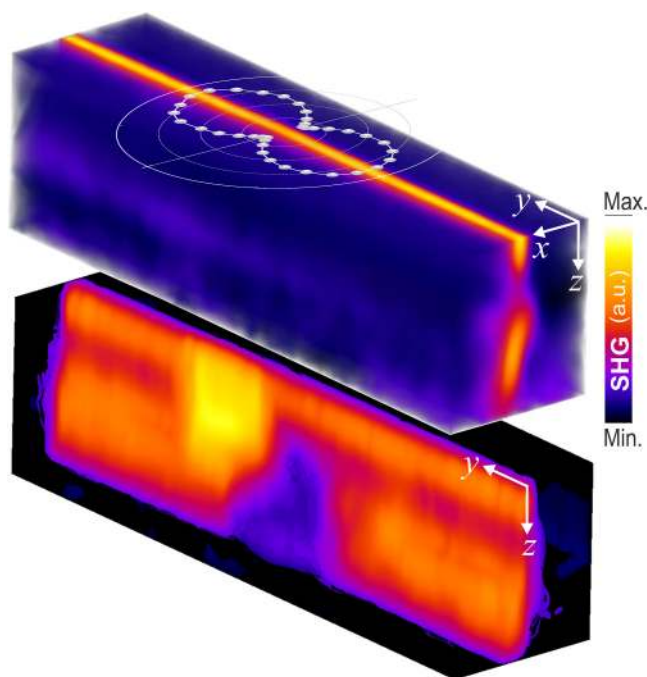


FIG. 8. Three-dimensional profile of a chiral Bloch-type wall showing a complex internal structure. The affixed polar plot represents the variation of the SHG intensity with the analyzer angle for a fundamental wave polarized along the wall. The color map represents the bulk SHG intensity in arbitrary units measured in a sample volume of $12 \times 55 \times 100 \mu\text{m}^3$. Adapted from Cherifi-Hertel *et al.*, Nat. Commun. **8**, 15768 (2017). Copyright 2017 Authors, licensed under a Creative Commons Attribution (CC BY 4.0) license.

constructed based on a stack of images measured at different depths of the sample (i.e., by measuring series of images at different distances between the objective lens and the sample). Figure 8 shows such an example of a 3D reconstruction of stacked images, displaying the 3D profile of a Bloch-type DW in nearly stoichiometric LiTaO₃. The modulation of the SHG signal in the 3D profile of the wall suggests a complex 3D wall structure involving both the wall distortion and a chirality transition. This structure is reminiscent of topological features known from magnetism. Bloch-type walls may exist in two variants since the ferroelectric polarization between *c*-domains of the opposite sign can rotate either clockwise or counterclockwise across the wall. The absence of mirror symmetry makes Bloch walls chiral. This property becomes particularly interesting if the chirality changes not only from one wall to another but also within the domain wall, as it is known to be possible in magnetic systems.¹⁷⁷ The transition regions separating Bloch walls with opposite chirality represent topological defects in the form of lines within the bulk of the magnetic crystals. Such line defects are known as Bloch lines. These 1D topological structures have inspired the design of original solid-state magnetic memory devices^{178,179} and have stimulated numerous studies among the magnetism community.^{180–183} It has been recently predicted that similar structures should also exist in ferroelectric¹⁸⁴

and ferroelastic^{57,185} systems. SHG does not allow for the discrimination between DW segments with antiparallel polarization because of its quadratic dependence on the susceptibility. However, the region between the two wall segments can show a Néel-like transition or zero polarization (called Ising line¹⁸⁴) leading to a different contrast with respect to the walls. This makes it possible to visualize Bloch lines in 3D SHG measurements.²⁴

V. SUMMARY AND OUTLOOK

The use of light, in particular, through the second-harmonic generation process, is a powerful means to detect and investigate local properties of polar DWs even though their size is far below the resolution limit of optical methods. The convolution of the probe beam with the comparatively zero size of the DWs makes it possible to observe SHG at non-centrosymmetric DWs. Their non-Ising character produces a unique spectral signature in SHG polarimetry experiments,^{23,24} which allows distinguishing between Néel-type and Bloch-type configurations.

The experimental studies on the internal structure of polar DWs are obviously inspired and supported by tremendous theoretical work that has been conducted on the subject. Several aspects predicted by theory still remain to be explored. Future experimental studies could, e.g., focus on the impact of the flexoelectric field on the chirality and the internal structure of polar twin boundaries^{186,187} and ferroelectric^{27,29,122} DWs, and attempt to evidence the link between the conductivity of ferroelectric DWs and their internal structure, as predicted by Morozovska⁴⁰ and Eliseev *et al.*¹⁸⁸ This would require the combination of different experiments with SHG microscopy polarimetry, like C-AFM, micro-diffraction, PFM, TEM, etc.

Experimental studies on the internal structure of DWs are also expected to assess theoretical models predicting their occurrence by exploring the range of validity of the models in terms of boundary conditions, temperature, pressure (strain), and surface vs bulk (3D) structure. Systematic experimental studies in which the effect of the external parameters on the internal structure of the walls are necessary to explain apparent discrepancies between theoretical predictions and experimental results and could be employed to specifically address the questions that are still unsettled in this context.

The recent development of new imaging modes to probe the non-linear optical response at the nanoscale shows great promise for the exploration of complex polar nanostructures. Rendón-Barraza *et al.*¹⁸⁹ have recently reported an SHG polarimetry study unraveling local crystalline aspects—at the sub-diffraction limit—in BaTiO₃ nanoparticles. This method can be adopted to resolve exotic polar topological structures predicted to arise in ferroelectric nanoparticles¹⁹⁰ such as vortices¹⁹¹ and Bloch points.¹⁹²

ACKNOWLEDGMENTS

This work was supported by the French National Research Agency (ANR) under Contract No. ANR-18-CE92-0052 through the TOPELEC project cofounded by the DFG under Grant No. EN-434/41-1. S.C.-H. and C.V. acknowledge funding by the LabEx NIE (ANR-11-LABX-0058_NIE) in the framework of the Interdisciplinary Thematic Institute QMat (ANR-17-EURE-

0024), as part of the ITI 2021-2028 program supported by the IdEx Unistra (ANR-10-IDEX-0002-002) and SFRI STRATUS (ANR-20-SFRI-0012) through the French Programme d'Investissement d'Avenir. S.C.-H is grateful to Gregory Taupier, Patrycja Paruch, Katia Gallo, and Lukas Eng for their close collaboration. This article summarizes results that have been published elsewhere, as cited in the text. Some of these previous results have been adapted and reused for didactic purposes.

DATA AVAILABILITY

The data that support the findings of this study are available from the corresponding author upon reasonable request.

REFERENCES

- ¹N. D. Mermin, *Rev. Mod. Phys.* **51**, 591 (1979).
- ²J. Seidel, R. K. Vasudevan, and N. Valanoor, *Adv. Electron. Mater.* **2**, 1500292 (2016).
- ³J. Seidel, *Nat. Mater.* **18**, 188 (2019).
- ⁴J. Seidel, in *Topological Structures in Ferroic Materials* (Springer International Publishing, Cham, 2016).
- ⁵D. A. Allwood, *Science* **309**, 1688 (2005).
- ⁶S. P. Parkin, M. Hayashi, and L. Thomas, *Science* **320**, 190 (2008).
- ⁷A. Fert, V. Cros, and J. Sampaio, *Nat. Nanotechnol.* **8**, 152 (2013).
- ⁸J.-Y. Chaudreau, T. Chirac, S. Fusil, V. Garcia, W. Akhtar, J. Tranchida, P. Thibaudau, I. Gross, C. Blouzon, A. Finco, M. Bibes, B. Dkhil, D. D. Khalyavin, P. Manuel, V. Jacques, N. Jaouen, and M. Viret, *Nat. Mater.* **19**, 386 (2020).
- ⁹I. I. Naumov, L. Bellaiche, and H. Fu, *Nature* **432**, 737 (2004).
- ¹⁰P. Shafer, P. García-Fernández, P. Aguado-Puente, A. R. Damodaran, A. K. Yadav, C. T. Nelson, S.-L. Hsu, J. C. Wojdel, J. Íñiguez, L. W. Martin, E. Arenholz, J. Junquera, and R. Ramesh, *Proc. Natl. Acad. Sci. U.S.A.* **115**, 915 (2018).
- ¹¹J. M. Gregg, *Ferroelectrics* **433**, 74 (2012).
- ¹²Y. Tikhonov, S. Kondovych, J. Mangeri, M. Pavlenko, L. Baudry, A. Sené, A. Galda, S. Nakhmanson, O. Heinonen, A. Razumnaya, I. Luk'yanchuk, and V. M. Vinokur, *Sci. Rep.* **10**, 8657 (2020).
- ¹³N. Strkalj, E. Gradauskaite, J. Nordlander, and M. Trassin, *Materials* **12**, 3108 (2019).
- ¹⁴S. Chen, S. Yuan, Z. Hou, Y. Tang, J. Zhang, T. Wang, K. Li, W. Zhao, X. Liu, L. Chen, L. W. Martin, and Z. Chen, *Adv. Mater.* **2000857**, e2000857 (2020).
- ¹⁵Y. Nahas, S. Prokhorenko, L. Louis, Z. Gui, I. Kornev, and L. Bellaiche, *Nat. Commun.* **6**, 8542 (2015).
- ¹⁶Z. Hong and L.-Q. Chen, *Acta Mater.* **152**, 155 (2018).
- ¹⁷M. A. Pereira Gonçalves, C. Escorihuela-Sayalero, P. Garca-Fernández, J. Junquera, and J. Íñiguez, *Sci. Adv.* **5**, eaau7023 (2019).
- ¹⁸S. Das, Y. L. Tang, Z. Hong, M. A. P. P. Gonçalves, M. R. McCarter, C. Klewe, K. X. Nguyen, F. Gómez-Ortiz, P. Shafer, E. Arenholz, V. A. Stoica, S.-L. Hsu, B. Wang, C. Ophus, J. F. Liu, C. T. Nelson, S. Saremi, B. Prasad, A. B. Mei, D. G. Schlom, J. Íñiguez, P. García-Fernández, D. A. Muller, L. Q. Chen, J. Junquera, L. W. Martin, and R. Ramesh, *Nature* **568**, 368 (2019).
- ¹⁹D. Meier, J. Seidel, M. Gregg, and R. Ramesh, *Domain Walls: From Fundamental Properties to Nanotechnology Concepts* (Oxford University Press, 2020).
- ²⁰J. Lajzerowicz and J. J. Niez, *J. Phys. Lett.* **40**, 165 (1979).
- ²¹V. Stepkova, P. Marton, and J. Hlinka, *J. Phys.: Condens. Matter* **24**, 212201 (2012).
- ²²X.-K. Wei, C.-L. Jia, T. Sluka, B.-X. Wang, Z.-G. Ye, and N. Setter, *Nat. Commun.* **7**, 12385 (2016).
- ²³G. De Luca, M. D. Rossell, J. Schaab, N. Viart, M. Fiebig, and M. Trassin, *Adv. Mater.* **29**, 1605145 (2017).
- ²⁴S. Cherifi-Hertel, H. Bulou, R. Hertel, G. Taupier, K. D. H. Dorkenoo, C. Andreas, J. Guyonnet, I. Gaponenko, K. Gallo, and P. Paruch, *Nat. Commun.* **8**, 15768 (2017).
- ²⁵J. Hlinka, V. Stepkova, P. Marton, I. Rychetsky, V. Janovec, and P. Ondrejko, *Phase Transitions* **84**, 738 (2011).
- ²⁶M. Taherinejad, D. Vanderbilt, P. Marton, V. Stepkova, and J. Hlinka, *Phys. Rev. B* **86**, 155138 (2012).
- ²⁷E. A. Eliseev, P. V. Yudin, S. V. Kalinin, N. Setter, A. K. Tagantsev, and A. N. Morozovska, *Phys. Rev. B* **87**, 054111 (2013).
- ²⁸B. Houchmandzadeh, J. Lajzerowicz, and E. Salje, *J. Phys.: Condens. Matter* **3**, 5163 (1991).
- ²⁹P. V. Yudin, A. K. Tagantsev, E. A. Eliseev, A. N. Morozovska, and N. Setter, *Phys. Rev. B* **86**, 134102 (2012).
- ³⁰D. Meier, *J. Phys.: Condens. Matter* **27**, 463003 (2015).
- ³¹P. Sharma, P. Schoenherr, and J. Seidel, *Materials* **12**, 2927 (2019).
- ³²D. M. Evans, V. Garcia, D. Meier, and M. Bibes, *Phys. Sci. Rev.* **5**, 9 (2020).
- ³³L. Goncalves-Ferreira, S. A. T. Redfern, E. Artacho, and E. K. H. Salje, *Phys. Rev. Lett.* **101**, 097602 (2008).
- ³⁴J. F. Scott, E. K. H. Salje, and M. A. Carpenter, *Phys. Rev. Lett.* **109**, 187601 (2012).
- ³⁵J. Seidel, L. W. Martin, Q. He, Q. Zhan, Y.-H. Chu, A. Rother, M. E. Hawkrigde, P. Maksymovych, P. Yu, M. Gajek, N. Balke, S. V. Kalinin, S. Gemming, F. Wang, G. Catalan, J. F. Scott, N. A. Spaldin, J. Orenstein, and R. Ramesh, *Nat. Mater.* **8**, 229 (2009).
- ³⁶S. Farokhipoor and B. Noheda, *Phys. Rev. Lett.* **107**, 127601 (2011).
- ³⁷J. Guyonnet, I. Gaponenko, S. Gariglio, and P. Paruch, *Adv. Mater.* **23**, 5377 (2011).
- ³⁸M. Schröder, A. Haußmann, A. Thiessen, E. Soergel, T. Woike, and L. M. Eng, *Adv. Funct. Mater.* **22**, 3936 (2012).
- ³⁹D. Meier, J. Seidel, A. Cano, K. Delaney, Y. Kumagai, M. Mostovoy, N. A. Spaldin, R. Ramesh, and M. Fiebig, *Nat. Mater.* **11**, 284 (2012).
- ⁴⁰A. N. Morozovska, *Ferroelectrics* **438**, 3 (2012).
- ⁴¹T. Sluka, A. K. Tagantsev, P. Bednyakov, and N. Setter, *Nat. Commun.* **4**, 1808 (2013).
- ⁴²J. Ma, J. Ma, Q. Zhang, R. Peng, J. Wang, C. Liu, M. Wang, N. Li, M. Chen, X. Cheng, P. Gao, L. Gu, L.-Q. Chen, P. Yu, J. Zhang, and C.-W. Nan, *Nat. Nanotechnol.* **13**, 947 (2018).
- ⁴³H. Lu, Y. Tan, J. P. V. McConville, Z. Ahmadi, B. Wang, M. Conroy, K. Moore, U. Bangert, J. E. Shield, L. Chen, J. M. Gregg, and A. Gruverman, *Adv. Mater.* **31**, 1902890 (2019).
- ⁴⁴L. Liu, K. Xu, Q. Li, J. Daniels, H. Zhou, J. Li, J. Zhu, J. Seidel, and J. Li, *Adv. Funct. Mater.* **31**, 2005876 (2021).
- ⁴⁵A. Aird and E. K. H. Salje, *J. Phys.: Condens. Matter* **10**, L377 (1998).
- ⁴⁶C. Stefani, L. Ponet, K. Shapovalov, P. Chen, E. Langenberg, D. G. Schlom, S. Artyukhin, M. Stengel, N. Domingo, and G. Catalan, *Phys. Rev. X* **10**, 041001 (2020).
- ⁴⁷J. Seidel, *J. Phys. Chem. Lett.* **3**, 2905 (2012).
- ⁴⁸G. Catalan, J. Seidel, R. Ramesh, and J. F. Scott, *Rev. Mod. Phys.* **84**, 119 (2012).
- ⁴⁹J. P. V. McConville, H. Lu, B. Wang, Y. Tan, C. Cochard, M. Conroy, K. Moore, A. Harvey, U. Bangert, L. Chen, A. Gruverman, and J. M. Gregg, *Adv. Funct. Mater.* **30**, 2000109 (2020).
- ⁵⁰X. Chai, J. Jiang, Q. Zhang, X. Hou, F. Meng, J. Wang, L. Gu, D. W. Zhang, and A. Q. Jiang, *Nat. Commun.* **11**, 2811 (2020).
- ⁵¹T. Kämpfe, B. Wang, A. Haußmann, L.-Q. Chen, and L. M. Eng, *Crystals* **10**, 804 (2020).
- ⁵²A. Q. Jiang, W. P. Geng, P. Lv, J. Hong, J. Jiang, C. Wang, X. J. Chai, J. W. Lian, Y. Zhang, R. Huang, D. W. Zhang, J. F. Scott, and C. S. Hwang, *Nat. Mater.* **19**, 1188 (2020).
- ⁵³J. Schaab, S. H. Skjærø, S. Krohns, X. Dai, M. E. Holtz, A. Cano, M. Lilienblum, Z. Yan, E. Bourret, D. A. Muller, M. Fiebig, S. M. Selbach, and D. Meier, *Nat. Nanotechnol.* **13**, 1028 (2018).
- ⁵⁴G. F. Nataf, M. Guennou, J. M. Gregg, D. Meier, J. Hlinka, E. K. H. Salje, and J. Kreisel, *Nat. Rev. Phys.* **2**, 634 (2020).
- ⁵⁵P. Zubko, G. Catalan, A. Buckley, P. R. L. Welche, and J. F. Scott, *Phys. Rev. Lett.* **99**, 167601 (2007).

- ⁵⁶E. K. H. Salje, O. Aktas, M. A. Carpenter, V. V. Laguta, and J. F. Scott, *Phys. Rev. Lett.* **111**, 247603 (2013).
- ⁵⁷E. K. H. Salje and J. F. Scott, *Appl. Phys. Lett.* **105**, 252904 (2014).
- ⁵⁸E. K. H. Salje, *J. Appl. Phys.* **128**, 164104 (2020).
- ⁵⁹C.-L. Jia, S.-B. Mi, K. Urban, I. Vrejoiu, M. Alexe, and D. Hesse, *Nat. Mater.* **7**, 57 (2008).
- ⁶⁰L. Li, P. Gao, C. T. Nelson, J. R. Jokisaari, Y. Zhang, S.-J. J. Kim, A. Melville, C. Adamo, D. G. Schlom, and X. Pan, *Nano Lett.* **13**, 5218 (2013).
- ⁶¹J. Gonnissen, D. Batuk, G. F. Nataf, L. Jones, A. M. Abakumov, S. Van Aert, D. Schryvers, and E. K. H. Salje, *Adv. Funct. Mater.* **26**, 7599 (2016).
- ⁶²J. Lee, *Curr. Appl. Phys.* **17**, 675 (2017).
- ⁶³J. F. Scott and A. Kumar, *Appl. Phys. Lett.* **105**, 052902 (2014).
- ⁶⁴A. Gruverman, M. Alexe, and D. Meier, *Nat. Commun.* **10**, 1 (2019).
- ⁶⁵J. Guyonnet, H. Béa, F. Guy, S. Gariglio, S. Fusil, K. Bouzehouane, J.-M. Triscone, and P. Paruch, *Appl. Phys. Lett.* **95**, 132902 (2009).
- ⁶⁶S. Cherifi, R. Hertel, S. Fusil, H. Béa, K. Bouzehouane, J. Allibe, M. Bibes, and A. Barthélémy, *Phys. Status Solidi* **4**, 22 (2010).
- ⁶⁷J. Schaab, I. P. Krug, F. Nickel, D. M. Gottlob, H. Doğanay, A. Cano, M. Hentschel, Z. Yan, E. Bourret, C. M. Schneider, R. Ramesh, and D. Meier, *Appl. Phys. Lett.* **104**, 232904 (2014).
- ⁶⁸J. Schaab, K. Shapovalov, P. Schoenherr, J. Hackl, M. I. Khan, M. Hentschel, Z. Yan, E. Bourret, C. M. Schneider, S. Nemsák, M. Stengel, A. Cano, and D. Meier, *Appl. Phys. Lett.* **115**, 122903 (2019).
- ⁶⁹G. F. Nataf, M. Guennou, J. Kreisel, P. Hicher, R. Haumont, O. Aktas, E. K. H. Salje, L. Tortech, C. Mathieu, D. Martinotti, and N. Barrett, *Phys. Rev. Mater.* **1**, 074410 (2017).
- ⁷⁰S. Kim and V. Gopalan, *Mater. Sci. Eng. B* **120**, 91 (2005).
- ⁷¹L. Kirsten, A. Haußmann, C. Schnabel, S. Schmidt, P. Cimalla, L. M. Eng, and E. Koch, *Opt. Express* **25**, 14871 (2017).
- ⁷²V. Gopalan, V. Dierolf, and D. A. Scrymgeour, *Annu. Rev. Mater. Res.* **37**, 449 (2007).
- ⁷³G. F. Nataf, M. Guennou, A. Haußmann, N. Barrett, and J. Kreisel, *Phys. Status Solidi* **10**, 222 (2016).
- ⁷⁴M. Rüsing, S. Neufeld, J. Brockmeier, C. Eigner, P. Mackwitz, K. Spychala, C. Silberhorn, W. G. Schmidt, G. Berth, A. Zrenner, and S. Sanna, *Phys. Rev. Mater.* **2**, 103801 (2018).
- ⁷⁵G. F. Nataf and M. Guennou, *J. Phys.: Condens. Matter* **32**, 183001 (2020).
- ⁷⁶A. Haußmann, L. M. Eng, and S. Cherifi-Hertel, in *Domain Walls*, edited by R. R. Dennis Meier, J. Seidel, and M. Gregg (Oxford University Press, 2020), pp. 152–184.
- ⁷⁷D. A. Bonnelli, D. N. Basov, M. Bode, U. Diebold, S. V. Kalinin, V. Madhavan, L. Novotny, M. Salmeron, U. D. Schwarz, and P. S. Weiss, *Rev. Mod. Phys.* **84**, 1343 (2012).
- ⁷⁸G. Tarrach, P. L. Lagos, R. Z. Hermans, F. Schlaphof, Ch. Loppacher, and L. M. Eng, *Appl. Phys. Lett.* **79**, 3152 (2001).
- ⁷⁹V. Ya. Shur and P. S. Zelenovskiy, *J. Appl. Phys.* **116**, 066802 (2014).
- ⁸⁰P. A. Franken, A. E. Hill, C. W. Peters, and G. Weinreich, *Phys. Rev. Lett.* **7**, 118 (1961).
- ⁸¹A. Kirilyuk, *J. Phys. D: Appl. Phys.* **35**, R189 (2002).
- ⁸²M. Fiebig, V. V. Pavlov, and R. V. Pisarev, *J. Opt. Soc. Am. B* **22**, 96 (2005).
- ⁸³S. A. Denev, T. T. A. Lummen, E. Barnes, A. Kumar, and V. Gopalan, *J. Am. Ceram. Soc.* **94**, 2699 (2011).
- ⁸⁴H. Yokota, J. Kaneshiro, and Y. Uesu, *Phys. Res. Int.* **2012**, 1 (2012).
- ⁸⁵M. Fiebig, T. Lottermoser, D. Fröhlich, A. V. Goltsev, and R. V. Pisarev, *Nature* **419**, 818 (2002).
- ⁸⁶M. Trassin, G. De Luca, S. Manz, and M. Fiebig, *Adv. Mater.* **27**, 4871 (2015).
- ⁸⁷J.-Y. Chauléau, E. Haltz, C. Carrétéro, S. Fusil, and M. Viret, *Nat. Mater.* **16**, 803 (2017).
- ⁸⁸J. Nordlander, G. De Luca, N. Strkalj, M. Fiebig, M. Trassin, and M. T. Id, *Appl. Sci.* **8**, 570 (2018).
- ⁸⁹J. Nordlander, F. Eltes, M. Reynaud, J. Nürnberg, G. De Luca, D. Caimi, A. A. Demkov, S. Abel, M. Fiebig, J. Fompeyrine, and M. Trassin, *Phys. Rev. Mater.* **4**, 34406 (2020).
- ⁹⁰M. F. Sarott, M. Fiebig, and M. Trassin, *Appl. Phys. Lett.* **117**, 132901 (2020).
- ⁹¹M. Flörsheimer, R. Paschotta, U. Kubitschek, C. Brillert, D. Hofmann, L. Heuer, G. Schreiber, C. Verbeek, W. Sohler, and H. Fuchs, *Appl. Phys. B Lasers Opt.* **67**, 593 (1998).
- ⁹²S. I. Bozhevolnyi, K. Pedersen, T. Skettrup, X. Zhang, and M. Belmonte, *Opt. Commun.* **152**, 221 (1998).
- ⁹³S. I. Bozhevolnyi, J. M. Hvam, K. Pedersen, F. Laurell, H. Karlsson, T. Skettrup, and M. Belmonte, *Appl. Phys. Lett.* **73**, 1814 (1998).
- ⁹⁴A. Fragemann, V. Pasiskevicius, and F. Laurell, *Appl. Phys. Lett.* **85**, 375 (2004).
- ⁹⁵X. Deng, H. Ren, H. Lao, and X. Chen, *J. Opt. Soc. Am. B* **27**, 1475 (2010).
- ⁹⁶X. Deng and X. Chen, *Opt. Express* **18**, 15597 (2010).
- ⁹⁷Y. Sheng, A. Best, H.-J. Butt, W. Krolikowski, A. Arie, and K. Koynov, *Opt. Express* **18**, 16539 (2010).
- ⁹⁸T. Kämpfe, P. Reichenbach, M. Schröder, A. Haußmann, L. M. Eng, T. Woike, and E. Soergel, *Phys. Rev. B* **89**, 035314 (2014).
- ⁹⁹H. Yokota, H. Usami, R. Haumont, P. Hicher, J. Kaneshiro, E. K. H. Salje, and Y. Uesu, *Phys. Rev. B* **89**, 144109 (2014).
- ¹⁰⁰H. Yokota, S. Matsumoto, E. K. H. Salje, and Y. Uesu, *Phys. Rev. B* **98**, 104105 (2018).
- ¹⁰¹H. Yokota, N. Hasegawa, M. Glazer, E. K. H. Salje, and Y. Uesu, *Appl. Phys. Lett.* **116**, 232901 (2020).
- ¹⁰²H. Yokota, C. R. S. Haines, S. Matsumoto, N. Hasegawa, M. A. Carpenter, Y. Heo, A. Marin, E. K. H. Salje, and Y. Uesu, *Phys. Rev. B* **102**, 104117 (2020).
- ¹⁰³L. E. Cross, *Advanced Ceramics III* (Springer Netherlands, Dordrecht, 1990), pp. 71–102.
- ¹⁰⁴H. Schmid, *J. Phys.: Condens. Matter* **20**, 434201 (2008).
- ¹⁰⁵R. Resta, *Ferroelectrics* **151**, 49 (1994).
- ¹⁰⁶L. D. Landau, L. P. Pitaevskii, and E. M. Lifshitz, *Electrodynamics of Continuous Media* (Butterworth-Heinemann, Oxford, 1995).
- ¹⁰⁷P. Weiss, *J. Phys. Théorique Appliquée* **6**, 661 (1907).
- ¹⁰⁸T. Mitsui and J. Furuichi, *Phys. Rev.* **90**, 193 (1953).
- ¹⁰⁹M. V. Klassen-Neklyudova, *Mechanical Twinning of Crystals* (Springer US, Boston, MA, 1964).
- ¹¹⁰L. Landau and E. Lifshitz, *Phys. Zeitsch. Der Sow.* **8**, 153 (1935).
- ¹¹¹C. Kittel, *Phys. Rev.* **70**, 965 (1946).
- ¹¹²G. Catalan, J. F. Scott, A. Schilling, and J. M. Gregg, *J. Phys.: Condens. Matter* **19**, 022201 (2006).
- ¹¹³I. A. Luk'yanchuk, L. Lahoche, and A. Sené, *Phys. Rev. Lett.* **102**, 147601 (2009).
- ¹¹⁴A. K. Tagantsev, L. E. Cross, and J. Fousek, *Domains in Ferroic Crystals and Thin Films* (Springer, New York, 2010).
- ¹¹⁵V. Y. Shur, E. V. Pelegova, and M. S. Kosobokov, *Ferroelectrics* **569**, 251 (2020).
- ¹¹⁶V. Y. Shur, A. R. Akhmatkhanov, and I. S. Baturin, *Appl. Phys. Rev.* **2**, 040604 (2015).
- ¹¹⁷V. Y. Shur, A. I. Lobov, A. G. Shur, E. L. Rumyantsev, and K. Gallo, *Ferroelectrics* **360**, 111 (2007).
- ¹¹⁸A. Hubert and R. Schäfer, *Magnetic Domains: The Analysis of Magnetic Microstructures* (Springer Berlin Heidelberg, New York, 2009).
- ¹¹⁹V. A. Zhirnov, *Sov. Phys. JETP* **8**, 822 (1959).
- ¹²⁰H. Kronmüller and M. Fähnle, *Micromagnetism and the Microstructure of Ferromagnetic Solids* (Cambridge University Press, Cambridge, 2003).
- ¹²¹R. K. Behera, C.-W. Lee, D. Lee, A. N. Morozovska, S. B. Sinnott, A. Asthagiri, V. Gopalan, and S. R. Phillpot, *J. Phys.: Condens. Matter* **23**, 175902 (2011).
- ¹²²Y. Gu, M. Li, A. N. Morozovska, Y. Wang, E. A. Eliseev, V. Gopalan, and L.-Q. Chen, *Phys. Rev. B* **89**, 174111 (2014).
- ¹²³J. C. Wojdel and J. Íñiguez, *Phys. Rev. Lett.* **112**, 247603 (2014).
- ¹²⁴D. A. Scrymgeour, V. Gopalan, A. Itagi, A. Saxena, and P. J. Swart, *Phys. Rev. B* **71**, 184110 (2005).
- ¹²⁵D. Lee, R. K. Behera, P. Wu, H. Xu, Y. L. Li, S. B. Sinnott, S. R. Phillpot, L. Q. Chen, and V. Gopalan, *Phys. Rev. B* **80**, 060102 (2009).

- ¹²⁶D. Lee, H. Xu, V. Dierolf, V. Gopalan, and S. R. Phillpot, *Phys. Rev. B* **82**, 014104 (2010).
- ¹²⁷A. Angoshtari and A. Yavari, *J. Appl. Phys.* **108**, 084112 (2010).
- ¹²⁸P. Marton, I. Rychetsky, and J. Hlinka, *Phys. Rev. B* **81**, 144125 (2010).
- ¹²⁹A. Grzybowski and K. Pietrzak, *Clin. Dermatol.* **31**, 221 (2013).
- ¹³⁰N. Bloembergen, *Nonlinear Optics* (Benjamin, New York, 1964).
- ¹³¹P. N. Butcher, *Nonlinear Optical Phenomena* (Ohio State University, 1965).
- ¹³²Y. R. Shen, *The Principles of Nonlinear Optics* (John Wiley & Sons, New York, 1984).
- ¹³³R. W. Boyd, *Nonlinear Optics* (Elsevier, 2003).
- ¹³⁴D. Sandkuijl, A. E. Tuer, D. Tokarz, J. E. Sipe, and V. Barzda, *J. Opt. Soc. Am. B* **30**, 382 (2013).
- ¹³⁵M. Gu, *Advanced Optical Imaging Theory* (Springer Berlin Heidelberg, Berlin, 2000).
- ¹³⁶L. Novotny and B. Hecht, *Principles of Nano-Optics* (Cambridge University Press, Cambridge, 2006).
- ¹³⁷J. Kaneshiro and Y. Uesu, *Jpn. J. Appl. Phys.* **50**, 09NE11 (2011).
- ¹³⁸D. Ait-Belkacem, A. Gasecka, F. Munhoz, S. Brustlein, and S. Brasselet, *Opt. Express* **18**, 14859 (2010).
- ¹³⁹E. Yew and C. Sheppard, *Opt. Express* **14**, 1167 (2006).
- ¹⁴⁰C.-L. Hsieh, Y. Pu, R. Grange, and D. Psaltis, *Opt. Express* **18**, 11917 (2010).
- ¹⁴¹K. J. Spychala, P. Mackwitz, A. Widhalm, G. Berth, and A. Zrenner, *J. Appl. Phys.* **127**, 023103 (2020).
- ¹⁴²K. J. Spychala, P. Mackwitz, M. Rüsing, A. Widhalm, G. Berth, C. Silberhorn, and A. Zrenner, *J. Appl. Phys.* **128**, 234102 (2020).
- ¹⁴³M. Rüsing, J. Zhao, and S. Mookherjee, *J. Appl. Phys.* **126**, 114105 (2019).
- ¹⁴⁴R. E. Newnham, *Properties of Materials*, 1st. ed. (Oxford University Press, 2005).
- ¹⁴⁵Y. Uesu, S. Kurimura, and Y. Yamamoto, *Appl. Phys. Lett.* **66**, 2165 (1995).
- ¹⁴⁶D. Meier, M. Maringer, T. Lottermoser, P. Becker, L. Bohaty, and M. Fiebig, *Phys. Rev. Lett.* **102**, 107202 (2009).
- ¹⁴⁷V. Gopalan and R. Raj, *Appl. Phys. Lett.* **68**, 1323 (1996).
- ¹⁴⁸Y. Barad, J. Lettieri, C. D. Theis, D. G. Schlom, and V. Gopalan, *J. Appl. Phys.* **90**, 3497 (2001).
- ¹⁴⁹E. D. Mishina, N. E. Sherstyuk, D. R. Barskiy, A. S. Sigov, Y. I. Golovko, V. M. Mukhorotov, M. De Santo, and Th. Rasing, *J. Appl. Phys.* **93**, 6216 (2003).
- ¹⁵⁰M. A. van der Veen, F. Vermoortele, D. E. De Vos, and T. Verbiest, *Anal. Chem.* **84**, 6378 (2012).
- ¹⁵¹J. Brandmüller, *Comput. Math. Appl.* **12**, 97 (1986).
- ¹⁵²J. Přívratská and V. Janovec, *Ferroelectrics* **191**, 17 (1997).
- ¹⁵³V. Janovec and V. Kopský, *Ferroelectrics* **191**, 23 (1997).
- ¹⁵⁴J. Přívratská and V. Janovec, *Ferroelectrics* **222**, 23 (1999).
- ¹⁵⁵P. Tolédano, M. Guennou, and J. Kreisel, *Phys. Rev. B* **89**, 134104 (2014).
- ¹⁵⁶W. Schranz, I. Rychetsky, and J. Hlinka, *Phys. Rev. B* **100**, 184105 (2019).
- ¹⁵⁷A. A. Bul'bich and Y. M. Gufan, *Sov. Phys. JETP* **67**, 1153 (1988).
- ¹⁵⁸T. A. Lummen, Y. Gu, J. Wang, S. Lei, F. Xue, A. Kumar, A. T. Barnes, E. Barnes, S. Denev, A. Belianinov, M. Holt, A. N. Morozovska, S. V. Kalinin, L.-Q. Chen, and V. Gopalan, *Nat. Commun.* **5**, 3172 (2014).
- ¹⁵⁹B. Liu, Y. Zheng, X. Zhao, H. Liu, and X. Chen, *Opt. Express* **24**, 29459 (2016).
- ¹⁶⁰H. Yokota, S. Matsumoto, N. Hasegawa, E. K. H. Salje, and Y. Uesu, *J. Phys.: Condens. Matter* **32**, 345401 (2020).
- ¹⁶¹M. Fiebig, D. Fröhlich, Th. Lottermoser, and M. Maat, *Phys. Rev. B* **66**, 144102 (2002).
- ¹⁶²G. Berth, V. Quiring, W. Sohler, and A. Zrenner, *Ferroelectrics* **352**, 78 (2007).
- ¹⁶³Y. J. Wang, D. Chen, Y. L. Tang, Y. L. Zhu, and X. L. Ma, *J. Appl. Phys.* **116**, 224105 (2014).
- ¹⁶⁴D. Mukherjee, S. Prokhorenko, L. Miao, K. Wang, E. Bousquet, V. Gopalan, and N. Alem, *Phys. Rev. B* **100**, 104102 (2019).
- ¹⁶⁵D. Li, X. Huang, Z. Xiao, H. Chen, L. Zhang, Y. Hao, J. Song, D.-F. Shao, E. Y. Tsybal, Y. Lu, and X. Hong, *Nat. Commun.* **11**, 1422 (2020).
- ¹⁶⁶Y. Uesu, H. Shibata, S. Suzuki, and S. Shimada, *Ferroelectrics* **304**, 99 (2004).
- ¹⁶⁷Y. Uesu, H. Yokota, S. Kawado, J. Kaneshiro, S. Kurimura, and N. Kato, *Appl. Phys. Lett.* **91**, 182904 (2007).
- ¹⁶⁸C. Godau, T. Kämpfe, A. Thiessen, L. M. Eng, and A. Haußmann, *ACS Nano* **11**, 4816 (2017).
- ¹⁶⁹A. Haußmann, L. Kirsten, S. Schmidt, P. Cimalla, L. Wehmeier, E. Koch, and L. M. Eng, *Ann. Phys.* **529**, 1700139 (2017).
- ¹⁷⁰A. A. Esin, A. R. Akhmatkhanov, and V. Y. Shur, *Appl. Phys. Lett.* **114**, 092901 (2019).
- ¹⁷¹B. Kirbus, C. Godau, L. Wehmeier, H. Beccard, E. Beyreuther, A. Haußmann, and L. M. Eng, *ACS Appl. Nano Mater.* **2**, 5787 (2019).
- ¹⁷²L. Wehmeier, T. Kämpfe, A. Haußmann, and L. M. Eng, *Phys. Status Solidi* **11**, 1700267 (2017).
- ¹⁷³V. D. Kugel and G. Rosenman, *Appl. Phys. Lett.* **62**, 2902 (1993).
- ¹⁷⁴T. Kämpfe, P. Reichenbach, A. Haußmann, T. Woike, E. Soergel, and L. M. Eng, *Appl. Phys. Lett.* **107**, 152905 (2015).
- ¹⁷⁵J. Ducuing and N. Bloembergen, *Phys. Rev. Lett.* **10**, 474 (1963).
- ¹⁷⁶Y. R. Shen, *Appl. Phys. B* **68**, 295 (1999).
- ¹⁷⁷J. C. Slonczewski, *J. Appl. Phys.* **45**, 2705 (1974).
- ¹⁷⁸S. Konishi, *IEEE Trans. Magn.* **19**, 1838 (1983).
- ¹⁷⁹L. Zimmermann, J. Miltat, and P. Pougnet, *IEEE Trans. Magn.* **27**, 5508 (1991).
- ¹⁸⁰A. Thiaville, J. Ben Youssef, Y. Nakatani, and J. Miltat, *J. Appl. Phys.* **69**, 6090 (1991).
- ¹⁸¹A. Thiaville, J. Miltat, and J. Ben Youssef, *Eur. Phys. J. B* **23**, 37 (2001).
- ¹⁸²T. Jourdan, A. Masseboeuf, F. Lançon, P. Bayle-Guillemaud, and A. Marty, *J. Appl. Phys.* **106**, 073913 (2009).
- ¹⁸³M. A. Borich, A. P. Tankeev, and V. V. Smagin, *Phys. Solid State* **58**, 1375 (2016).
- ¹⁸⁴V. Stepkova, P. Marton, and J. Hlinka, *Phys. Rev. B* **92**, 094106 (2015).
- ¹⁸⁵E. K. H. Salje and M. A. Carpenter, *Phys. Status Solidi* **252**, 2639 (2015).
- ¹⁸⁶A. Schiaffino and M. Stengel, *Phys. Rev. Lett.* **119**, 137601 (2017).
- ¹⁸⁷A. N. Morozovska, E. A. Eliseev, M. D. Glinchuk, L.-Q. Chen, and V. Gopalan, *Phys. Rev. B* **85**, 094107 (2012).
- ¹⁸⁸E. A. Eliseev, A. N. Morozovska, G. S. Svechnikov, P. Maksymovych, and S. V. Kalinin, *Phys. Rev. B* **85**, 045312 (2012).
- ¹⁸⁹C. Rendón-Barraza, F. Timpu, R. Grange, and S. Brasselet, *Sci. Rep.* **9**, 1670 (2019).
- ¹⁹⁰A. N. Morozovska, Y. M. Fomichov, P. Maksymovych, Y. M. Vysochanskii, and E. A. Eliseev, *Acta Mater.* **160**, 109 (2018).
- ¹⁹¹J. Mangeri, Y. Espinal, A. Jokisaari, S. Pamir Alpay, S. Nakhmanson, and O. Heinonen, *Nanoscale* **9**, 1616 (2017).
- ¹⁹²A. N. Morozovska, E. A. Eliseev, R. Hertel, Y. M. Fomichov, V. Tulaidan, V. Y. Reshetnyak, and D. R. Evans, *Acta Mater.* **200**, 256 (2020).